Posted on 30 Oct 2022 — The copyright holder is the author/funder. All rights reserved. No reuse without permission. — https://doi.org/10.22541/au.166709885.56047528/v1 — This a preprint and has not been peer reviewed. Data may be preliminary.

Synergistic effects of herbal compounds to promote osteoporotic fracture repair through upregulation of β-catenin signaling in skeletal muscle satellite cells

Zhenxiong Jin[1], Weiwei Da[2], Chen Huang[1], Yong-Jian Zhao[1], Tengteng Wang[1], Hao Xu[1], Hongbo Wan[1], Xiang Gao[3], Xuequn Wu[1], Qi Shi[1], Yong-Jun Wang[1], and Dezhi Tang[1]

[1]Shanghai University of Traditional Chinese Medicine
[2]Shanghai Medical Hospital of Traditional Chinese Medicine
[3]Huadong Hospital Affiliated to Fudan University

October 30, 2022

Abstract

Background and purpose: Osteoporotic fracture (OPF) disrupts the balance of bone formation by osteoblasts and bone resorption by osteoclasts. we found that compounds from herbal medicine, Invigorate the Spleen and Tonify the Kidney Formula (ISTKF) accelerates fracture healing. Identification of the active ingredients in ISFKF and the mechanisms of fracture healing involved was carried out. Experimental approach: Using $\Pi a\xi 7\text{-}\tilde{\gamma}\rho\epsilon^{EPT2/+}\cdot\beta\text{-}\varsigma a\tau\epsilon\nu\iota\nu^{\varphi\xi/\varphi\xi}$ conditional knockout(cKO) mice, the mechanisms involved in promoting fracture healing were assessed by looking at the fracture site and its surrounding muscle tissue, using various experiments to analyze the signaling involved. The key molecules and compounds involved in this fracture-promoting effect were identified by HPLC analysis. Key results: Histopathological staining of muscles and micro-CT of bone revealed that β-catenin knockout in skeletal muscle satellite cells (SMSCs) gives rise to sarcopenia and osteopenia, and ISTKF significantly promoted muscle firmness and also increased proliferation and osteogenic differentiation of SMSCs. ISTKF inhibits the significant decrease in bone mass and the destruction of bone microstructure in $\Pi a\xi 7\text{-}\tilde{\gamma}\rho\epsilon^{EPT2/+}\cdot\beta\text{-}\varsigma a\tau\epsilon\nu\iota\nu^{\varphi\xi/\varphi\xi}$ cKO mice. ISTKF mediates the β-catenin signaling pathway to mobilize SMSCs to migrate to the fracture site, promotes the osteogenic differentiation of SMSCs, and promotes the activity of cartilage and osteoblasts at the OPF site. When β-catenin is promoted by ISTKF, it promotes skeletal muscle fiber remodeling and fractures healing. Conclusion and implications: These results provided the first practical evidence for ISTKF-mediated regulation of SMSCs via β-catenin to promote fracture healing with clinical implications that would aid in the treatment of delayed healing and nonunion of fractures.

The data that support the findings of this study are available from the corresponding author upon reasonable request. Some data may not be made available because of privacy or ethical restrictions.

Synergistic effects of herbal compounds to promote osteoporotic fracture repair through upregulation of β-catenin signaling in skeletal muscle satellite cells

Zhenxiong Jin [a,b], Weiwei Da [c], Chen Huang [a,b,d], Yongjian Zhao [a,b], Tengteng Wang [a], Hao Xu [a,b], Hongbo Wan [a], Xiang Gao [e], Xuequn Wu [a], Qi Shi [a,b], Yongjun Wang [a,b,d], Dezhi Tang [a,b]*

[a] Longhua Hospital, Shanghai University of Traditional Chinese Medicine, Shanghai 200032, China

[b] Institute of Spine, Shanghai University of Traditional Chinese Medicine, Shanghai 200032, China

[c] Department of Orthopedics, Shanghai Medical Hospital of Traditional Chinese Medicine, Shanghai 200071, China

[d] Shanghai University of Traditional Chinese Medicine, Shanghai 201203, China

[e] Department of Surgery, Huadong Hospital Affiliated to Fudan University, Shanghai 200040, China

*** Corresponding Author:**

Dezhi Tang, Longhua Hospital, Shanghai University of Traditional Chinese Medicine, 725 Wan-Ping South Road, Shanghai 200032, China; E-mail: dztang702@126.com

Running title: ISTKF Activates the SMSCs to Promote OPF Repair by β-catenin

Abstract

Background and purpose: Osteoporotic fracture (OPF) disrupts the balance of bone formation by osteoblasts and bone resorption by osteoclasts. we found that compounds from herbal medicine, Invigorate the Spleen and Tonify the Kidney Formula (ISTKF) accelerates fracture healing. Identification of the active ingredients in ISFKF and the mechanisms of fracture healing involved was carried out.

Experimental approach: Using *Pax7-Cre*$^{ERT2/+}$;*β-catenin*$^{fx/fx}$ conditional knockout(cKO) mice, the mechanisms involved in promoting fracture healing were assessed by looking at the fracture site and its surrounding muscle tissue, using various experiments to analyze the signaling involved. The key molecules and compounds involved in this fracture-promoting effect were identified by HPLC analysis.

Key results: Histopathological staining of muscles and micro-CT of bone revealed that β-catenin knockout in skeletal muscle satellite cells (SMSCs) gives rise to sarcopenia and osteopenia, and ISTKF significantly promoted muscle firmness and also increased proliferation and osteogenic differentiation of SMSCs. ISTKF inhibits the significant decrease in bone mass and the destruction of bone microstructure in *Pax7-Cre*$^{ERT2/+}$;*β-catenin*$^{fx/fx}$ cKO mice. ISTKF mediates the β-catenin signaling pathway to mobilize SMSCs to migrate to the fracture site, promotes the osteogenic differentiation of SMSCs, and promotes the activity of cartilage and osteoblasts at the OPF site. When β-catenin is promoted by ISTKF, it promotes skeletal muscle fiber remodeling and fractures healing.

Conclusion and implications: These results provided the first practical evidence for ISTKF-mediated regulation of SMSCs via β-catenin to promote fracture healing with clinical

implications that would aid in the treatment of delayed healing and nonunion of fractures.

Keywords: osteoporotic fracture; skeletal muscle stem cells; fracture healing; osteoblast; *β*-catenin

Abbreviations

OPF, Osteoporotic fracture; ISTKF, Invigorate the Spleen and Tonify the Kidney Formula; TCM, Traditional Chinese Medicine; MyoD, myogenic differentiation; Pax7, paired box 7; cKO, conditional gene knockout; micro-CT, micro-computed tomography; BMD, bone mineral density; dpf, days post-fracture; BSA, bovine serum albumin; H&E, hematoxylin and eosin; ABHO, Alcian blue/hematoxylin & Orange G; BV/TV, bone volume/total volume; Tb. N, number of trabecular bone; Tb. Th, thickness of trabecular bone; OPG, osteoprotegerin; RANK; receptor activator of nuclear factor-kB; RANKL, RANK Ligand; CP, Codonopsis pilosula; RD, Rhizoma drynariae; AS, Acanthopanax senticosus; EBM, Epimedium brevicornum Maxim; SMB, Slauia miltiorrhiza Bunge; RAP, root of Angelicae pubescens; BrdU, 5-Bromo-2-deoxyUridine; Sca1, stem cell antigen-1; MAPK, mitogen-activated protein kinase; ROS, reactive oxygen species; ARE, antioxidant response element.

Bullet point summary:

What is already known

• Osteoporotic fracture is one of most serious and common complications of osteoporosis.

• There is no effective pharmacological therapy for this disease at present.

What this study adds

• β-catenin knockout in skeletal muscle satellite cells (SMSCs) gives rise to sarcopenia and osteopenia

• ISTKF mediates the β-catenin signalling pathway and mobilises SMSCs to the fracture side to promote fracture healing.

What is the clinical significance

• ISTKF and its active ingredient may offer a new approach to the treatment of delayed healing and non-union of fractures

1 | INTRODUCTION

Osteoporotic fractures (OPF), also known as fragility fractures, are one of the most common diseases worldwide (Rapp *et al.*, 2022). The balance between bone resorption and formation is conducive to maintaining skeletal integrity and is strictly regulated by osteoclasts, osteoblasts, and osteocytes (Langdahl, 2021). The disruption of this balance leads to pathological changes in bone quality and structure (Fujii *et al.*, 2021; Raggatt *et al.*, 2010). In 2017, 2.68 million new fragility fractures were estimated in France, Germany, Italy, Spain, Sweden, and the United Kingdom (Adams *et al.*, 2021), indicating that by 2040, more than 300 million adults ≥ 50 years old will be at high risk of osteoporotic fracture globally (Oden *et al.*, 2015). Although surgery is the main treatment strategy for osteoporotic fractures because it reduces the risk of death for many patients and improves physical functioning, little is known about its impact on social costs (Gu *et al.*, 2014). Given this imminent economic and social burden, improving the treatment of high-risk groups of osteoporotic fractures would help to develop complete intervention strategies.

The Invigorate the Spleen and Tonify the Kidney Formula (ISTKF) is the result of over sixty years of clinical experience in the treatment of degenerative bone diseases by Professor Shi of the Shanghai University of Traditional Chinese Medicine (TCM). Combined with the TCM theory of "spleen and kidney treatment simultaneously" (Xiong *et al.*, 2019) and "strengthening bones and muscles" (Wu *et al.*, 2013), we clarified the analysis of the curative effect and the mechanism of promoting fracture healing based on the correlation between muscles and bones. In a previous study, we found that the ISTKF mobilized skeletal muscle satellite cells (SMSCs) to promote the healing of ovariectomized OPF mice and found that ISTKF significantly accelerates the healing of OPF (Da *et al.*, 2017). The mechanism may be that it upregulates the activity of some SMSCs,

increases the expression of β-catenin (Wang *et al.*, 2014; Yan *et al.*, 2009), and promotes its osteogenic multidirectional differentiation to participate in fracture repair (Tang *et al.*, 2010). On the other hand, it reduces the fracture healing time by balancing the correlation between osteoclasts and osteoblasts (Tang *et al.*, 2011; Da, 2016). Therefore, adjusting the muscle and bones can promote the healing of OPF.

Potentially, β-catenin signaling is altered in patients with muscle defects, such as myopathy and atrophy, due to genetic defects or epigenetic factors (Alexander *et al.*, 2013; Suzuki *et al.*, 2018). Specifically, β-catenin interacts with myogenic differentiation (MyoD) and binds to and activates the target genes (Kim *et al.*, 2008). SMSCs are attached to the muscle fibers between the sarcolemma and the basement membrane (Li *et al.*, 2019). Typically, they are in a static state, but after stimulation, such as pluripotent stem cells, they exhibit pluripotent mesenchymal stem cell activity (Cornelison, 2018; Wang *et al.*, 2011). The paired box 7 (Pax7) is a critical molecular marker of SMSCs that determines the formation of SMSCs during embryogenesis (Corona *et al.*, 2016). Reportedly, (Montarras *et al.*, 2013; Xiang *et al.*, 2012) SMSCs also differentiate into osteoblasts, but only a few studies have been conducted on this aspect.

Therefore, the present study used *Pax7-Cre*$^{ERT2/+}$*;β-catenin*$^{fx/fx}$ cKO mice to knock out β-catenin in SMSCs. In vivo experiments revealed the correlation between muscle and bone and the changes caused by ISTKF on bone and muscle of cKO mice were observed. The present study aimed to illustrate the role of ISTKF on β-catenin to regulate SMSCs in fracture healing.

2 | METHODS

2.1 | Preparation of ISTKF

Herbs in ISTKF (Table 1) were identified by the pharmacists of Longhua Hospital Affiliated with

the Shanghai University of TCM, following standard protocol. According to the Chinese Pharmacopoeia, all crude drugs were soaked in 12 volumes of water for 30 min and boiled for 40 min. The extracts were filtered, the filter residues were boiled in 8 volumes of water for another 40 min, and then the solution was filtered again. Two batches of drug filtrates were mixed and prepared for intragastric administration.

2.2 | Other Reagents

Strong bone capsule (cat. #Z20030007) was purchased from Beijing Qihuang Pharmaceutical Co., Ltd (Beijing, China); RIPA lysis buffer (cat. #P0013B), SDS-PAGE protein loading buffer(cat. #P0015L), BeyoECL star (cat. #P0018AS), SDS-PAGE electrophoresis buffer (cat. #P0014D), SDS-PAGE kit (cat. #P0012AC), and Western Transfer Film (cat. #P0021B) were from Beyotime (Shanghai China); MASSON kit (cat. #G1006) and GD fixative (cat. #G1111) were from Servicebio (Wuhan, China); anti-GAPDH antibody (cat. #ab181602), anti-β-catenin antibody (cat. #ab6302), goat anti-rabbit (cat. #ab205718), anti-BrdU antibody (cat. #ab6326), anti-Sca1 antibody (cat. #ab25031), and anti-Pax7 antibody (cat. #ab187339) were from Abcam (UK); anti-MYOD antibody was purchased from Novus (UK) (cat. #NBP1-54153); Tamoxifen (cat. #T5648), *Clostridium histolyticum* (cat. #C6885), eosin (cat. #E4009-5G), hematoxylin (cat. #H-3136), Alcian Blue (cat.#A5268), Orange G (cat. #1936-15-8), Phloxine B (cat. #18472-87-2), dimethyl sulfoxide (DMSO) (Sigma Amresco cat. #67-68-5), albumin bovine V (Sigma Roche cat. #10735078001), and trypsin (cat. #T7409) were from Sigma (USA); ABC-HRP Kit (cat. #PK-6100), Antifade Mounting Medium with DAPI (cat. #H-1200), and DAB Substrate Kit (cat. #SK-4100) were from Vector Labs (USA); anti-rabbit IgG (H+L) 555 (cat. #4413/4409) and anti-rat IgG (H+L) 488 (cat. #4413) were from Cell Signaling Technology (CST) (USA).

2.3 | *Pax7 Cre$^{ERT2/+}$;β-catenin$^{fx/fx}$* Mice

β-catenin$^{fx/fx}$ and *Pax7 Cre$^{ERT2/+}$* mice were generated as described previously and maintained on C57BL/6J background. *Pax7 Cre$^{ERT2/+}$* mice were crossed with *β-catenin$^{fx/fx}$* mice to obtain *Pax7 Cre$^{ERT2/+}$;β-catenin$^{fx/fx}$ mice* (C57BL/6J). The genotype was determined by polymerase chain reaction (PCR) on tail genomic DNA from 3-week-old mice. Primer sequences were available upon request. The mice were randomly divided into the *Pax7 Cre$^{ERT2/+}$;β-catenin$^{fx/fx}$* group (TM group) and the *β-catenin$^{fx/fx}$* group (Con group). The animal protocols were reviewed and approved by the Shanghai University of TCM on animal care (Ethics Review Number: PZSHUTCM190329005). Animal studies are reported following ARRIVE guidelines(Kilkenny *et al.*, 2010) and recommendations of the *British Journal of Pharmacology.*

2.4 | Model Establishment and Evaluation of Osteoporosis

For postnatal activation of Pax7 Cre, 100 mg/kg tamoxifen in corn oil was intraperitoneally injected into 1-month-old TM group mice once a day for 5 consecutive days. In a preliminary study, the micro-computed tomography (micro-CT) scans of the tibia of the TM and Con groups were compared. Consequently, we found that after knocking out the β-catenin in SMSCs, the TM group mice exhibited a significant decrease in bone mineral density (BMD) (***P<0.001, Supplemental Figure 1A). Also, the bone microstructure of the tibial plateau was destroyed.

2.5 | Construction of an OPF Model

First, 3-month-old mice of the TM and Con groups were anesthetized intraperitoneally with ketamine hydrochloride. The mice were placed in a supine position, the hair from their calf was removed and disinfected with iodine, and the skin was cut 1.5 cm through the left anterior tibia under aseptic conditions. Second, the fascia and muscles on the medial and lateral parts of the

upper tibia were bluntly separated. The Kirschner wire was inserted from the tibial plateau into the upper one-third of the tibia. Then, the tibia was transected. Third, the Kirschner wire was inserted into the bone cavity at the lower end of the broken end, and the part that leaked out of the bone was cut off. Finally, the skin was sutured layer by layer.

2.6 | Experimental Groups

A total of 20 litter-negative *β-catenin*$^{fx/fx}$ mice comprised the Con-Vehicle group and 60 *Pax7 Cre*$^{ERT2/+}$*;β-catenin*$^{fx/fx}$ mice were randomly divided into TM-Vehicle, TM-Formula, and TM-Positive. Each group was assessed at two time points, 7 and 14 days post-fracture (dpf), with 10 mice in each group at each time point.

According to the "Methods of Pharmacology of New Chinese Medicines," the formula for the conversion of doses between mice and humans was as follows: the dose of mice=1/70*10*weight*number*day. According to one dose per day for adults, mice need 7 and 14 days, and each mouse was administered 0.2 mL/day by gavage. From the second day after the establishment of the tibial fracture model, the Formula group was treated with ISTKF, the Positive group was treated with a Strong bone Capsule, and the Vehicle group was treated with an equivalent volume of 0.9% normal saline. All mice had free access to water.

2.7 | Immunohistochemical Staining

After routine dewaxing, the sections were immersed in methanol: H_2O_2 (1:9) for 15 min, followed by antigen retrieval with collagenase from *Clostridium histolyticum*. The sections were blocked with 5% bovine serum albumin (BSA) at room temperature for 20 min and incubated with primary rabbit antibodies against β-catenin (β-catenin: 1% BSA 1:200) at 4℃ overnight, followed by goat anti-rabbit IgG at 37 ℃ for 15 min. Then, the avidin/biotin enzyme complex horseradish

peroxidase was added dropwise at room temperature for 15 min. The complex was visualized using a 3,3'-diaminobenzidine color development solution, and the sections were observed under Olympus VS120-SL at 20X magnification. The immune-related procedures used are per the recommendations of the British Journal of Pharmacology (Alexander *et al.*, 2018).

2.8 | Western Blot

The antibody-based procedures used in this study are by the recommendations of the *British Journal of Pharmacology* (Alexander *et al.*, 2018). After the final treatment, all the mice were sacrificed. The weight of the posterior tibial muscle was measured immediately after extraction and preserved at -80 ℃. Subsequently, the protein was extracted and estimated using the BCA method; the extract was stored at -20 °C. An equivalent of protein was separated by 8–12% SDS-PAGE and transferred to the PVDF membrane. After blocking in 5% BSA in PBST at room temperature for 1 h, the membrane was probed with the corresponding primary antibodies (β-catenin 1:4000, MyoD1 1:4000, MEF2C 1:4000, GAPDH 1:4000) in 1% BSA, at 4 °C overnight. Then, the membrane was probed with the corresponding secondary antibody (1:1000/1:10000) diluted with 1% BSA and incubated at room temperature for 2 h. Subsequently, the immunoreactive bands were visualized.

2.9 | Immunofluorescent Staining

After routine dewaxing, then antigen retrieval was performed with collagenase from *Clostridium histolyticum*. The sections were blocked with 5% BSA at room temperature for 20 min. Primary rabbit antibodies were used to visualize Pax7 (Pax7:1% BSA 1:200) + BrdU (BrdU:1% BSA 1:200), MyoD (MyoD:1% BSA 1:200) + BrdU (BrdU:1% BSA 1:200), Pax7 (Pax7:1% BSA 1:200) + Sca1 (Sca1:1% BSA 1:200) at 4℃ overnight. Then, anti-rabbit IgG (488:5% BSA 1:500

+ 555:5% BSA 1:500) was added. The cells were stained in the dark at room temperature for 1 h. The nuclei were counterstained with DAPI and examined under Olympus VS120-SL 20X filter (green, blue, and ultraviolet).

2.10 | Histopathological Examination

Muscle tissues were fixed with GD fixative for 24 h. The soft tissues were dehydrated, embedded in paraffin, and sliced into sagittal and horizontal serial sections (4-μm-thick). The decalcified femoral sections were stained with H&E and Masson's, and analyzed using Olympus VS120-SL. Simultaneously, 14% ethylenediaminetetraacetic acid (pH 7.4) was applied for decalcification for 3–4 weeks. After confirming the decalcification by X-ray, the sections were subjected to dehydration and paraffin embedding, followed by sagittal serial sectioning (4-μm-thick). Decalcified tibia sections were stained with hematoxylin and eosin (H&E), Alcian blue/hematoxylin & Orange G (ABHO), and Safranin-fixed green, and immunofluorescence and immunohistochemical staining. After full-length scanning, the target area of the ankle talus was analyzed using Olympus VS120-SL image analysis software.

2.11 | X-ray and micro-CT

The left tibia was carefully dissected and cleared of the adjacent muscle before immersing in 10% neutral formalin for 24 h. The formalin was replaced with 75% ethanol for long-term fixation, and a micro-CT scan was performed for uniform positioning. The left upper tibia was one-third, and the resolution was 18 μm. The X-ray (55 kVp, 71 μA) of the left tibia was. The quantitative analysis of bone tissue morphology assessed bone volume/total volume (BV/TV), the number of trabecular bone (Tb. N), and thickness of trabecular bone (Tb. Th).

2.12 | HPLC-Q-TOF of ISTKF

The components of ISTKF were characterized on an Agilent 1290 UPLC Ultra Performance Liquid Chromatograph (Agilent Co., USA) connected to an Agilent Q-TOF 6545 LC/MS high-resolution tandem mass spectrometer (Agilent Co., USA). The operating parameters were optimized in both positive and negative modes as follows: gas temperature (325 °C), drying gas (8 L/min), nebulizer (45 psi), shealth gas temperature (325 °C), shealth gas flow (8 L/min), Vcap (4000 V), nozzle voltage (1000 V), fragmentor (175 V), skimmer (V), and collision energy (40 eV). The compounds in ISTKF were separated on a Waters CORTECS®UPLC® T3 (2.1×100 mm, 1.6 μm). The mobile phase was composed of solvent A (acetonitrile) and solvent B (water containing 0.1% formic acid); the flow rate was 0.3 mL/min. The gradient elution was as follows: 0–5 min: 0% A, 100% B; 5–10 min: 0–10% A, 100–90% B; 10–15 min: 10–15% A, 90–85% B; 15–35 min: 15–35% A, 85–65% B; 35–40 min: 35–70% A, 65–30% B; 40–43 min: 70–90% A, 30–10% B; 43–47 min: 90% A, 10% B; 47–47.1 min: 90–0% A, 10–100% B; 47.1–50 min: 0% A, 100% B. The column temperature was maintained at 30 ℃. The system operations and data analysis were conducted on MassHunter Workstation Software Qualitative Analysis (version B.07.00).

2.13 | Statistical Analysis

The data and statistical analysis are in line with the *British Journal of Pharmacology* recommendations for the design and analysis of pharmacology experiments (Curtis *et al.*, 2018). All data were presented as mean±standard error of the mean. The sample sizes were calculated assuming that a 30% difference in the parameters measured is biologically significant with an estimate of 10–20% of the expected mean. Alpha and beta were set to the standard values of 0.05 and 0.8, respectively. No animals or samples were excluded from the analysis, and animals were

randomized to Con-Vehicle, TM-Vehicle, TM-Formula, and TM-Positive, respectively. For comparisons of four groups, the one-way analysis of variance and least-significant difference test was used if the data passed the normality tests; otherwise, the Kruskal-Wallis test was used, followed by Dunn's multiple comparison test. SPSS 24.0 statistical software was used for statistical analysis. A *P*-value <0.05 was considered statistically significant (**P*<0.05, ***P*<0.01, and ****P*<0.001). GraphPad Prism 8 was used as the drawing software.

2.14 | Nomenclature of targets and ligands

Key protein targets and ligands in this article are hyperlinked to corresponding entries in http://www.guidetopharmacology.org, the common portal for data from the IUPHAR/BPS Guide to PHARMACOLOGY (Harding *et al.*, 2018), and are permanently archived in the Concise Guide to PHARMACOLOGY 2021/22 (Alexander *et al.*, 2021; Alexander *et al.*, 2021; Alexander *et al.*, 2021).

3 | Results

3.1 | ISTKF mediates β-catenin to promote myogenic differentiation

According to the mouse muscle wet weight coefficient ratio, the muscle wet weight ratio of the TM-Vehicle group decreased significantly compared to the Con-Vehicle group after drug intervention for 7 dpf (****P*<0.001). The comparison between the three groups of TM did not differ markedly. At 14 dpf, the TM-Formula and TM-Positive groups showed an increased muscle-wet-weight ratio compared to the TM-Vehicle group. The TM-Formula group had a significant effect compared to the TM-Vehicle group (**P*<0.05). This phenomenon showed that ISTKF upregulates the wet weight of muscles, which is improved after β-catenin knockout but does not exceed that of the Con-Vehicle group, indicating that the β-catenin signaling pathway is

one of the major signaling pathways of ISTKF (Figure 1A and 1B).

Muscle β-catenin immunohistochemical staining showed that the protein expression in the TM three groups was significantly lower than that in the Con-Vehicle group. At 14 dpf, the β-catenin expression of ISTKF was upregulated in the muscle, but that in the three TM groups was significantly lower than that of the Con-Vehicle group, confirming efficient gene knockout (Figure 1C and 1D). In addition, Western blot analysis of the posterior tibial muscle revealed that the expression of β-catenin in the three TM groups was significantly lower than that in the Con-Vehicle group (***P<0.001), indicating that the gene knockout efficiency was efficient. At 14 dpf, both the TM-Formula and TM-Positive groups were promoted, but the effect of the TM-Formula group was not as obvious as that of the TM-Positive group. Consecutively, the detection of myogenic differentiation indicators MyoD1 and MEF2C showed that at 14 dpf, both the TM-Formula and the TM-Positive groups improved; the effect in the TM-Formula group was most significant (Figure 1E and 1F). The immunofluorescence staining of muscle revealed that the treatment of ISTKF promotes the expression of MyoD and 5-Bromo-2-deoxyUridine (BrdU), indicating enhanced proliferation of muscle cells and the repair of muscle damage, but the effect is similar to the Con-Vehicle group (Figure 1G and Supplemental Figure 2A).

3.2 | ISTKF mediates β-catenin to regulate SMSCs and promotes myogenic differentiation

The H&E staining of the horizontal and sagittal planes of the muscles showed that at 7 dpf, the muscles of the TM-Vehicle, TM-Formula, and TM-Positive groups are relaxed. Conversely, the muscles are tighter in the Con-Vehicle group than in the first three groups. At 14 dpf, the muscle relaxation of the TM-Formula and TM-Positive groups improved, but it was not better than in the

Con-Vehicle group (Figure 2A and 2B). In addition, Masson's staining in the horizontal and sagittal planes of the muscles showed that there was no significant difference in the distribution of collagen fibers in 7 dpf, while at 14 dpf, the distribution of the TM-Formula group was more obvious than that of the TM-Vehicle group. This result indicated that ISTKF promotes muscle firmness and the formation of collagen fibers in the vicinity of the fracture (Figure 2C and 2D). Simultaneously, Pax7 is a critical molecular marker of SMSCs that determines the formation of satellite cells during embryonic development. Pax7 + BrdU and Pax7 + stem cell antigen-1 (Sca1) staining showed that the expression of SMSC in ISTKF was increased significantly but was not obvious Con in the TM three groups (Figure 2E-2F and Supplemental Figure 1B-1C). This finding showed that β-catenin is one of the main ways to promote the proliferation and differentiation of muscle and SMSCs by ISTKF.

3.3 | ISTKF mediates β-catenin to promote OPF healing

At 7 dpf, X-rays found that each group had a clear fracture line. At 14 dpf, TM-Vehicle had no obvious callus connection at the broken end; the fracture line began to blur in the Con-Vehicle group, and a large number of calluses were formed at the fracture end and crossed the fracture line; the TM-Formula and TM-Positive groups show only a partial improvement (Figure 3A). Micro-CT showed that at 7 dpf, the three-dimensional (3D) reconstruction image can be observed intuitively and is not markedly different from the reconstruction image. However, quantitative analysis showed that the BV/TV of the TM-Vehicle group was significantly lower compared to the Con-Vehicle group (Figure 3B). At 14 dpf, the 3D reconstruction of the Con-Vehicle group showed obvious callus formation, while the TM-Formula and TM-Positive groups showed a small improvement, albeit not significantly. Quantitative analysis revealed that compared to the

Con-Vehicle group, the BV/TV of the TM-Vehicle group was significantly lower (***P<0.001). Compared to the TM-Vehicle group, the TM-Formula and TM-Positive groups had statistically significant differences in the Conn-Dens and Tb.Th (**P<0.01; *P<0.05), but none of them exceeded the Con-Vehicle group (Figure 3C).

Additionally, H&E staining revealed that the fractured end of the Con-Vehicle, TM-Formula, and TM-Positive groups began to form a callus, but no obvious callus was formed at the fractured end of the TM-Vehicle group at 7 dpf (Figure 3D). The cartilage callus in the TM-Formula and TM-Positive groups increased gradually, and the callus in the Con-Vehicle group began to take shape, but the TM-Vehicle group had no obvious callus formation at 14 dpf (Figure 3E). The ABHO staining showed that at 7 dpf, there was no obvious cartilage formation in the TM-Vehicle group, while the Con-Vehicle, TM-Formula, and TM-Positive groups had a large amount of cartilage hyperplasia at the fracture site (Figure 3F). At 14 dpf, the cartilage began to increase in the TM-Formula and TM-Positive groups, while that in the Con-Vehicle group increased significantly; the TM-Vehicle group did not exhibit a large amount of cartilage formation (Figure 3G). Finally, Safranin-fixed Green staining results were similar to those of ABHO. At 7 dpf, no obvious cartilage was formed in the TM-Vehicle group, while that at the fractured end proliferated markedly in the Con-Osthole group (Figure 3H). At 14 dpf, cartilage increased significantly in the TM-Formula and TM-Positive groups. Also, the cartilage is in the Con-Vehicle group, but no obvious cartilage was formed in the TM-Vehicle group (Figure 3I). The pathological staining of H&E, ABHO, and Safranin-fixed Green found that knocking out β-catenin in SMSCs resulted in the obvious delay in the formation of callus, cartilage, and osteogenesis in mice. However, the treatment with ISTKF can partially accelerate the healing of OPF, but it is not better than the

Con-Vehicle group.

3.4 | ISTKF mediates β-catenin to regulate osteogenic differentiation of SMSCs and promote OPF healing

Immunohistochemical staining of osteoprotegerin (OPG) revealed that at 7 dpf, the callus area in the Con-Vehicle group was visible and the OPG-positive staining in the cytoplasm was significantly different from that in the TM-Vehicle, TM-Formula, and TM-Positive groups (***P<0.001). At 14 dpf, the TM-Formula and TM-Positive groups were significantly higher than the TM-Vehicle group (***P<0.001; Figure 4A). Double immunofluorescence staining showed the SMSC-specific protein gene (Pax7) and surface antigen (Sca1) in the tibial callus, indicating that ISTKF promotes the expression of SMSCs at the fracture site at 14 dpf. In the TM-Vehicle group, only Pax7, and not Sca1, was expressed, thereby indicating that the ISTKF upregulates the expression of SMSCs in damaged muscles in the early stage, but the effect is not better than that of the Con-Vehicle group (Figure 4B). In addition, the double staining of Pax7 and proliferation (BrdU) expression revealed that ISTKF promotes the proliferation of SMSCs at 14 dpf. The expression of SMSCs was significantly higher than that of the TM-Vehicle group, indicating that ISTKF promotes the proliferation activity of SMSCs, but the effect is not similar to that of the Con-Vehicle group (Figure 4C). This finding indicated that β-catenin is one of the main signaling pathways for the treatment of OPF to promote the proliferation and differentiation of SMSCs by ISTKF.

3.5 | Active Compound Analysis by ISTKF

The active compound analysis of ISTKF was measured by HPLC-Q-TOF, and illustrated in the following schematics: Representative ion chromatogram of ISTK in the negative mode (Figure

5A); Representative ion chromatogram of ISTK in the positive mode (Figure 5B). The analysis results showed 44 detection peaks in the ISTKF (Table 2). Among them, 27 compounds were definitively identified by comparison with the standard compounds, while the remaining 17 compounds were tentatively characterized according to their formula, retention time, and fragmentation patterns. Among them, the main ones from *Slauia miltiorrhiza Bunge* are Caffeic acid 3-O-β-D-glucoside, Salvianolic acid B, and 15 other compounds; The main compounds from *Epimedium brevicornum Maxim* are Icariin, Magnoflorine and 11 others; The main ones from *Root of Angelicae Pubescens* include 9 compounds such as Osthole and Angenomalin; The main compounds from *Codonopsis pilosula* include 5 compounds such as Codonopsine and Chlorogenic acid; The main compounds from *Rhizoma Drynariae* include 3 compounds such as Naringin and Neoeriocitrin; The main compounds from *Acanthopanax senticosus* are Eleutheroside B2 and Eleutheroside E.

4 | Discussion

In this study, we proved that ISTKF inhibits the significant decrease in bone mass and the destruction of bone microstructure in *Pax7-Cre$^{ERT2/+}$;β-catenin$^{fx/fx}$* cKO mice. We also found that ISTKF mediates the β-catenin signaling pathway to mobilize SMSCs to migrate to the fracture site, promotes the osteogenic differentiation of SMSCs, and promotes the activity of cartilage and osteoblasts at the OPF site. On the other hand, it promotes the function of the spleen and stomach, improves the absorption of the compound, and participates in the repair of the muscles around the fracture end, jointly accelerating the healing of OPF. Interestingly, β-catenin knockout in SMSCs gives rise to sarcopenia and osteopenia. On the contrary, when β-catenin is promoted by ISTKF, it promotes fracture healing and skeletal muscle fiber remodeling. Therefore, ISTKF regulates

SMSCs to exert a critical role in β-catenin-mediated osteoporotic fracture healing (**Figure 6**).

The specific composition and efficacy of ISTKF are as follows. *Codonopsis pilosula* (CP) is a perennial herbaceous plant in the genus *Codonopsis* of Campanulaceae and belongs to the spleen and lung meridian. It has been shown to have various pharmacological effects, such as anti-tumor, anti-microbial, antioxidant, and immune-enhancing properties (Wan *et al.*, 2020; Zou *et al.*, 2019); *Rhizoma drynariae* (RD) is a plant of the order Rhizoma Drynariae of the Rhizoma Drynariae family., which belong to the kidney and liver meridian. Its effective components can inhibit bone resorption or stimulate bone formation by regulating the targets of signal pathways, such as OPG/receptor activator of nuclear factor-κB (RANK)/RANK Ligand (RANKL), Wnt/β-catenin, and bone morphogenetic protein (BMP), and ultimately achieve the goal of preventing and treating osteoporosis. (Wan *et al.*, 2020; Zou *et al.*, 2019). *Acanthopanax senticosus* (AS) is a plant of Umbelliferae of the Araliaceae family; it belongs to the spleen, kidney, and heart meridian, prevents bone loss by inhibiting the RANK signaling pathway, inhibits osteoclast production induced by RANKL, and may be used to treat osteoclast-related diseases (Xu *et al.*, 2020). *Epimedium brevicornum* Maxim (EBM) is a perennial herb of the Berberis family, which has the functions of nourishing the kidney and strengthening yang, muscles, and bones. Also, it has potential anti-osteoporosis activity and may be an active ingredient that stimulates osteoblasts (Meng *et al.*, 2005; Zheng *et al.*, 2020). *Slauia miltiorrhiza* Bunge (SMB) is a plant of the Lamiaceae, which has bitterness and is slightly cold. It belongs to the heart and liver meridians and has been identified as having anti-cancer, antioxidant, anti-fibrosis, and anti-inflammatory properties (Nagappan *et al.*, 2019). The root of *Angelicae pubescens* (RAP) is the dried root of the Umbelliferae plant *Angelica sinensis*, which belongs to the kidney and bladder meridian. It has a

wide range of biological activities, such as anti-inflammatory, osteogenic, anti-fungal, and insecticidal, and has been used to treat rheumatism, pain, fever, and back pain (Yuan *et al.*, 2020).

Our previous studies have shown that ISTKF upregulates the expression of β-catenin and promotes the positive expression of OPG in the callus (Da *et al.*, 2017). Simultaneously, SMSCs are mobilized to migrate to the callus and promote the proliferation of chondrocytes at the fractured end in the early stage, promote the apoptosis of chondrocytes in the middle stage, and increase the number of osteoblasts (Da, 2016). And SMSCs have been shown to mediate the role of β-catenin in promoting osteoporotic fracture healing to improve our understanding of the role of SMSCs in promoting fracture healing and allow us to explore their potential as therapeutic targets (Jin *et al.*, 2022). At the same time, osthole, the active ingredient of ISPKF, can attenuate osteoclast formation by stimulating the activation of β-catenin-OPG signaling (Jin *et al.*, 2021). Compared to previous studies, in the present study, for the first time, conditional knockout mice have been applied to test the effects of this classic herbal compound and determine the underlying mechanisms.

However, using ISTKF for intervention, it was found that OPF healing was improved in the TM-Formula group but was not similar to that in the Con-vehicle group, indicating that ISTKF promotes fracture healing through the β-catenin signaling pathway and other channels. Some studies demonstrated that miR-122 inhibits the proliferation and differentiation of osteoblasts in osteoporotic rats (Meng *et al.*, 2020), and BMP signaling operates during routine satellite cell function to coordinate the balance between proliferation and differentiation before Noggin is activated to antagonize BMPs and facilitate terminal differentiation (Ono *et al.*, 2011). In addition, some scholars have shown that ARC could potentially inhibit osteoclastogenesis by abrogating

receptor activator of nuclear factor-κB ligand (RANKL)-induced mitogen-activated protein kinase (MAPK), calcium, and NFATc1 signaling pathway, as well as by promoting the expression of reactive oxygen species (ROS) scavenging enzymes in Nrf2/Keap1/antioxidant response element (ARE) signaling pathway (Ono *et al.*, 2011). Furthermore, epidermal growth factor receptor (Liu *et al.*, 2019), growth differentiation factor 11-fat mass and obesity-associated protein axis (Shen *et al.*, 2018), nuclear factor-kappa B, mitogen-activated protein kinases (M peroxisome proliferator-activated receptor gamma APK) (Wang *et al.*, 2020), protein kinase B (Liu *et al.*, 2016), vitamin D (Donato *et al.*, 2020), and other signaling pathways promote the fracture healing in osteoporotic bone. Moreover, oxidative stress and inflammation (Wang *et al.*, 2013) might promote fracture healing, which requires an in-depth exploration. And, through systematic review analysis, we found that bone mesenchymal stem cells could accelerate callus maturity, ossification and restore the mechanical properties of bones in osteoporotic fractures (Wang *et al.*, 2013). These studies have opened a new avenue for the treatment of OPFs and provided a basis for future clinical applications.

Further studies are needed to clarify the pharmacokinetics of ISTKF to provide references for optimal dosage and clinical indications. Currently, a large number of factors are detected in this TCM compound, and even the proportion of the compound needs to be optimized. Therefore, we must first prove the effectiveness of ISTKF in vitro and in vivo. These mechanisms provide direction for the follow-up studies. We also plan to continue exploring other signaling pathways through network pharmacology in future studies.

In summary, after treatment with ISTKF, the muscle wet weight coefficient of the OPF model of *Pax7-Cre*$^{ERT2/+}$*;β-catenin*$^{fx/fx}$ conditional gene knockout mice can be significantly improved. It

promotes the firmness of the muscles and the formation of collagen fibers in the vicinity of fractures. In addition, ISTKF promotes the proliferation activity of SMSCs, thereby promoting the formation of calli, which accelerates the healing time of fractures. Although ISTKF improved, knocking out β-catenin in SMSCs was not better than that in the Con-vehicle group, indicating that the β-catenin signaling pathway is one of the main mechanisms underlying ISTKF-regulated SMSCs to treat OPF.

ETHICAL STANDARDS

The animal study was reviewed and approved by the Shanghai University of Traditional Chinese Medicine: Animal Ethics Committee. Ethics Review Number: PZSHUTCM190329005.

ACKNOWLEDGEMENTS

This study was sponsored by research grants from the National Natural Science Foundation (81973883,81730107), the National Key R&D Program of China (2018YFC1704300), the Shanghai Scientific Research Project (20S21902000), the Innovation Team and Talents Cultivation Program of the National Administration of Traditional Chinese Medicine (ZYYCXTD-C-202202), and the Innovation Team of the Ministry of Education (IRT1270).

AUTHOR CONTRIBUTIONS

DZT and YJW designed and interpreted the experiments. QS provided theoretical guidance. ZXJ, WWD, CH and HBW executed the experiments. ZXJ and YJZ acquired and analyzed data. TTW and XQW aided the experiments. HX and XG provided reagents. ZXJ and DZT wrote the manuscript. All authors were involved in the writing and critical review of the manuscript and approved the final version for submission.

CONFLICT OF INTEREST

The authors have declared that no conflict of interest exists.

DECLARATION OF TRANSPARENCY AND SCIENTIFIC RIGOUR

This Declaration acknowledges that this paper adheres to the principles for transparent reporting and scientific rigour of preclinical research as stated in the BJP guidelines for Design & Analysis, Immunoblotting, Immunochemistry, and Animal Experimentation, and as recommended by funding agencies, publishers, and other organizations engaged with supporting research.

REFERENCES

Adams, J, Wilson, N, Hurkmans, E, Bakkers, M, Balazova, P, Baxter, M, Blavnsfeldt, AB, Briot, K, Chiari, C, Cooper, C, Dragoi, RG, Gabler, G, Lems, W, Mosor, E, Pais, S, Simon, C, Studenic, P, Tilley, S, de la Torre-Aboki, J, Stamm, TA (2021) 2019 EULAR points to consider for non-physician health professionals to prevent and manage fragility fractures in adults 50 years or older. *ANN RHEUM DIS* **80**(1)**:** 57-64.

Alexander, MS, Kawahara, G, Motohashi, N, Casar, JC, Eisenberg, I, Myers, JA, Gasperini, MJ, Estrella, EA, Kho, AT, Mitsuhashi, S, Shapiro, F, Kang, PB, Kunkel, LM (2013) MicroRNA-199a is induced in dystrophic muscle and affects WNT signaling, cell proliferation, and myogenic differentiation. *CELL DEATH DIFFER* **20**(9)**:** 1194-1208.

Alexander, S, Roberts, RE, Broughton, B, Sobey, CG, George, CH, Stanford, SC, Cirino, G, Docherty, JR, Giembycz, MA, Hoyer, D, Insel, PA, Izzo, AA, Ji, Y, MacEwan, DJ, Mangum, J, Wonnacott, S, Ahluwalia, A (2018) Goals and practicalities of immunoblotting and immunohistochemistry: A guide for submission to the British Journal of Pharmacology. *Br J Pharmacol* **175**(3)**:** 407-411.

Alexander, SP, Christopoulos, A, Davenport, AP, Kelly, E, Mathie, A, Peters, JA, Veale, EL, Armstrong, JF, Faccenda, E, Harding, SD, Pawson, AJ, Southan, C, Davies, JA, Abbracchio, MP, Alexander, W, Al-Hosaini, K, Back, M, Barnes, NM, Bathgate, R, Beaulieu, JM, Bernstein, KE, Bettler, B, Birdsall, N, Blaho, V, Boulay, F, Bousquet, C, Brauner-Osborne, H, Burnstock, G, Calo, G, Castano, JP, Catt, KJ, Ceruti, S, Chazot, P, Chiang, N, Chini, B, Chun, J, Cianciulli, A, Civelli, O, Clapp, LH, Couture, R, Csaba, Z, Dahlgren, C, Dent, G, Singh, KD, Douglas, SD, Dournaud, P, Eguchi, S, Escher, E, Filardo, EJ, Fong, T, Fumagalli, M, Gainetdinov, RR, Gasparo, M, Gerard, C, Gershengorn, M, Gobeil, F, Goodfriend, TL, Goudet, C, Gregory, KJ, Gundlach, AL, Hamann, J, Hanson, J, Hauger, RL, Hay, DL, Heinemann, A, Hollenberg, MD, Holliday, ND, Horiuchi, M, Hoyer, D, Hunyady, L, Husain, A, IJzerman, AP, Inagami, T, Jacobson, KA, Jensen, RT, Jockers, R, Jonnalagadda, D, Karnik, S, Kaupmann, K, Kemp, J, Kennedy, C, Kihara, Y, Kitazawa, T, Kozielewicz, P, Kreienkamp, HJ, Kukkonen, JP, Langenhan, T, Leach, K, Lecca, D, Lee, JD,

Leeman, SE, Leprince, J, Li, XX, Williams, TL, Lolait, SJ, Lupp, A, Macrae, R, Maguire, J, Mazella, J, McArdle, CA, Melmed, S, Michel, MC, Miller, LJ, Mitolo, V, Mouillac, B, Muller, CE, Murphy, P, Nahon, JL, Ngo, T, Norel, X, Nyimanu, D, O'Carroll, AM, Offermanns, S, Panaro, MA, Parmentier, M, Pertwee, RG, Pin, JP, Prossnitz, ER, Quinn, M, Ramachandran, R, Ray, M, Reinscheid, RK, Rondard, P, Rovati, GE, Ruzza, C, Sanger, GJ, Schoneberg, T, Schulte, G, Schulz, S, Segaloff, DL, Serhan, CN, Stoddart, LA, Sugimoto, Y, Summers, R, Tan, VP, Thal, D, Thomas, WW, Timmermans, P, Tirupula, K, Tulipano, G, Unal, H, Unger, T, Valant, C, Vanderheyden, P, Vaudry, D, Vaudry, H, Vilardaga, JP, Walker, CS, Wang, JM, Ward, DT, Wester, HJ, Willars, GB, Woodruff, TM, Yao, C, Ye, RD (2021) THE CONCISE GUIDE TO PHARMACOLOGY 2021/22: G protein-coupled receptors. *Br J Pharmacol* **178 Suppl 1:** S27-S156.

Alexander, SP, Kelly, E, Mathie, A, Peters, JA, Veale, EL, Armstrong, JF, Faccenda, E, Harding, SD, Pawson, AJ, Southan, C, Buneman, OP, Cidlowski, JA, Christopoulos, A, Davenport, AP, Fabbro, D, Spedding, M, Striessnig, J, Davies, JA, Ahlers-Dannen, KE, Alqinyah, M, Arumugam, TV, Bodle, C, Dagner, JB, Chakravarti, B, Choudhuri, SP, Druey, KM, Fisher, RA, Gerber, KJ, Hepler, JR, Hooks, SB, Kantheti, HS, Karaj, B, Layeghi-Ghalehsoukhteh, S, Lee, JK, Luo, Z, Martemyanov, K, Mascarenhas, LD, McNabb, H, Montanez-Miranda, C, Ogujiofor, O, Phan, H, Roman, DL, Shaw, V, Sjogren, B, Sobey, C, Spicer, MM, Squires, KE, Sutton, L, Wendimu, M, Wilkie, T, Xie, K, Zhang, Q, Zolghadri, Y (2021) THE CONCISE GUIDE TO PHARMACOLOGY 2021/22: Introduction and Other Protein Targets. *Br J Pharmacol* **178 Suppl 1:** S1-S26.

Alexander, SP, Kelly, E, Mathie, A, Peters, JA, Veale, EL, Armstrong, JF, Faccenda, E, Harding, SD, Pawson, AJ, Southan, C, Davies, JA, Amarosi, L, Anderson, C, Beart, PM, Broer, S, Dawson, PA, Hagenbuch, B, Hammond, JR, Inui, KI, Kanai, Y, Kemp, S, Stewart, G, Thwaites, DT, Verri, T (2021) THE CONCISE GUIDE TO PHARMACOLOGY 2021/22: Transporters. *Br J Pharmacol* **178 Suppl 1:** S412-S513.

Chen, D, Ye, Z, Wang, C, Wang, Q, Wang, H, Kuek, V, Wang, Z, Qiu, H, Yuan, J, Kenny, J, Yang, F, He, J, Liu, Y, Wang, G, Zhang, M, Zhang, G, Wang, J, Chen, P, Xu, J (2020) Arctiin abrogates osteoclastogenesis and bone resorption via suppressing RANKL-induced ROS and NFATc1 activation. *PHARMACOL RES* **159:** 104944.

Cornelison, D (2018) "Known Unknowns": Current Questions in Muscle Satellite Cell Biology. *CURR TOP DEV BIOL* **126:** 205-233.

Corona, BT, Greising, SM (2016) Challenges to acellular biological scaffold mediated skeletal muscle tissue regeneration. *BIOMATERIALS* **104:** 238-246.

Curtis, MJ, Alexander, S, Cirino, G, Docherty, JR, George, CH, Giembycz, MA, Hoyer, D, Insel, PA, Izzo, AA, Ji, Y, MacEwan, DJ, Sobey, CG, Stanford, SC, Teixeira, MM, Wonnacott, S, Ahluwalia, A (2018) Experimental design and analysis and their reporting II: updated and simplified guidance for authors and peer reviewers. *Br J Pharmacol* **175**(7)**:** 987-993.

Da, W. W. (2016). Study on Invigorate the Spleen and Tonify the Kidney Formula and its effective components in regulating osteogenic differentiation of myogenic stem cells and promoting osteoporotic fracture healing. Shanghai University of Traditional Chinese Medicine.(CHINA).

Da, W. W., Zhao, Y. J., Lan, R. X., Wang, T. T., Tang, D. Z., Shu, B., et al. (2017). Effect of Invigorate the Spleen and Tonify the Kidney Formula to increase the expression of β-catenin and Runx2 to promote the healing of osteoporotic fractures. Chinese Journal of Osteoporosis, *23*(06), 719-726.(CHINA).

Donato, AA, Nesfeder, J (2020) Supplementation with vitamin D plus calcium reduces fracture risk; vitamin D alone does not. *ANN INTERN MED* **172**(10)**:** C51.

Fujii, T, Murata, K, Mun, SH, Bae, S, Lee, YJ, Pannellini, T, Kang, K, Oliver, D, Park-Min, KH, Ivashkiv, LB (2021) MEF2C regulates osteoclastogenesis and pathologic bone resorption via c-FOS. *BONE RES* **9**(1)**:** 4.

Gu, Q, Koenig, L, Mather, RR, Tongue, J (2014) Surgery for hip fracture yields societal benefits that exceed the direct medical costs. *Clin Orthop Relat Res* **472**(11)**:** 3536-3546.

Harding, SD, Sharman, JL, Faccenda, E, Southan, C, Pawson, AJ, Ireland, S, Gray, A, Bruce, L, Alexander, S, Anderton, S, Bryant, C, Davenport, AP, Doerig, C, Fabbro, D, Levi-Schaffer, F, Spedding, M, Davies, JA (2018) The IUPHAR/BPS Guide to PHARMACOLOGY in 2018: updates and expansion to encompass the new guide to IMMUNOPHARMACOLOGY. *NUCLEIC ACIDS RES* **46**(D1)**:** D1091-D1106.

Jin, Z, Chen, J, Shu, B, Xiao, Y, Tang, D (2019) Bone mesenchymal stem cell therapy for ovariectomized osteoporotic rats: a systematic review and meta-analysis. *BMC Musculoskelet Disord* **20**(1)**:** 556.

Jin, Z, Da, W, Zhao, Y, Wang, T, Xu, H, Shu, B, Gao, X, Shi, Q, Ma, Y, Zhang, Y, Wang, Y, Tang, D (2022) Role of skeletal muscle satellite cells in the repair of osteoporotic fractures mediated by beta-catenin. *J Cachexia Sarcopenia Muscle* **13**(2)**:** 1403-1417.

Jin, ZX, Liao, XY, Da, WW, Zhao, YJ, Li, XF, Tang, DZ (2021) Osthole enhances the bone mass of senile osteoporosis and stimulates the expression of osteoprotegerin by activating beta-catenin signaling. *STEM CELL RES THER* **12**(1)**:** 154.

Kilkenny, C, Browne, W, Cuthill, IC, Emerson, M, Altman, DG (2010) Animal research: reporting in vivo experiments: the ARRIVE guidelines. *Br J Pharmacol* **160**(7)**:** 1577-1579.

Kim, CH, Neiswender, H, Baik, EJ, Xiong, WC, Mei, L (2008) Beta-catenin interacts with MyoD and regulates its transcription activity. *MOL CELL BIOL* **28**(9)**:** 2941-2951.

Langdahl, BL (2021) Overview of treatment approaches to osteoporosis. *Br J Pharmacol* **178**(9)**:**

1891-1906.

Li, L, Cheng, X, Chen, L, Li, J, Luo, W, Li, C (2019) Long Noncoding Ribonucleic Acid MSTRG.59589 Promotes Porcine Skeletal Muscle Satellite Cells Differentiation by Enhancing the Function of PALLD. *FRONT GENET* **10:** 1220.

Liu, G, Xie, Y, Su, J, Qin, H, Wu, H, Li, K, Yu, B, Zhang, X (2019) The role of EGFR signaling in age-related osteoporosis in mouse cortical bone. *The FASEB Journal* **33**(10)**:** 11137-11147.

Liu, H, Liu, Z, Du J, He, J, Lin, P, Amini, B, Starbuck, MW, Novane, N, Shah, JJ, Davis, RE, Hou, J, Gagel, RF, Yang, J (2016) Thymidine phosphorylase exerts complex effects on bone resorption and formation in myeloma. *SCI TRANSL MED* **8**(353)**:** 113r-353r.

Meng, FH, Li, YB, Xiong, ZL, Jiang, ZM, Li, FM (2005) Osteoblastic proliferative activity of Epimedium brevicornum Maxim. *PHYTOMEDICINE* **12**(3)**:** 189-193.

Meng, Y, Lin, T, Jiang, H, Zhang, Z, Shu, L, Yin, J, Ma, X, Wang, C, Gao, R, Zhou, X (2020) miR-122 Exerts Inhibitory Effects on Osteoblast Proliferation/Differentiation in Osteoporosis by Activating the PCP4-Mediated JNK Pathway. *Molecular Therapy - Nucleic Acids* **20:** 345-358.

Montarras, D, L'Honore, A, Buckingham, M (2013) Lying low but ready for action: the quiescent muscle satellite cell. *FEBS J* **280**(17)**:** 4036-4050.

Nagappan, A, Kim, JH, Jung, DY, Jung, MH (2019) Cryptotanshinone from the Salvia miltiorrhiza Bunge Attenuates Ethanol-Induced Liver Injury by Activation of AMPK/SIRT1 and Nrf2 Signaling Pathways. *INT J MOL SCI* **21**(1).

Oden, A, McCloskey, EV, Kanis, JA, Harvey, NC, Johansson, H (2015) Burden of high fracture probability worldwide: secular increases 2010-2040. *Osteoporos Int* **26**(9)**:** 2243-2248.

Ono, Y, Calhabeu, F, Morgan, JE, Katagiri, T, Amthor, H, Zammit, PS (2011) BMP signalling permits population expansion by preventing premature myogenic differentiation in muscle satellite cells. *CELL DEATH DIFFER* **18**(2)**:** 222-234.

Raggatt, LJ, Partridge, NC (2010) Cellular and molecular mechanisms of bone remodeling. *J BIOL CHEM* **285**(33)**:** 25103-25108.

Rapp, K, Lamb, SE, Roigk, P, Becker, C, Konnopka, C, Konig, HH, Peter, RS, Rothenbacher, D, Buchele, G (2022) Effect of an osteoporotic fracture prevention program on fracture incidence in routine care: a cluster-randomized trial. *BMC MED* **20**(1)**:** 49.

Shen, GS, Zhou, HB, Zhang, H, Chen, B, Liu, ZP, Yuan, Y, Zhou, XZ, Xu, YJ (2018) The GDF11-FTO-PPARgamma axis controls the shift of osteoporotic MSC fate to adipocyte and inhibits bone formation during osteoporosis. *Biochim Biophys Acta Mol Basis Dis* **1864**(12)**:**

3644-3654.

Suzuki, A, Minamide, R, Iwata, J (2018) WNT/β-catenin signaling plays a crucial role in myoblast fusion through regulation of nephrin expression during development. *DEVELOPMENT* **145**(23)**:** v168351.

Tang, DZ, Hou, W, Zhou, Q, Zhang, M, Holz, J, Sheu, TJ, Li, TF, Cheng, SD, Shi, Q, Harris, SE, Chen, D, Wang, YJ (2010) Osthole stimulates osteoblast differentiation and bone formation by activation of beta-catenin-BMP signaling. *J BONE MINER RES* **25**(6)**:** 1234-1245.

Tang, DZ, Yang, F, Yang, Z, Huang, J, Shi, Q, Chen, D, Wang, YJ (2011) Psoralen stimulates osteoblast differentiation through activation of BMP signaling. *Biochem Biophys Res Commun* **405**(2)**:** 256-261.

Wan, L, Zhang, Q, Luo, H, Xu, Z, Huang, S, Yang, F, Liu, Y, Mahaman, Y, Ke, D, Wang, Q, Liu, R, Wang, JZ, Shu, X, Wang, X (2020) Codonopsis pilosula polysaccharide attenuates Abeta toxicity and cognitive defects in APP/PS1 mice. *Aging (Albany NY)* **12**(13)**:** 13422-13436.

Wang, B, Jin, H, Zhu, M, Li, J, Zhao, L, Zhang, Y, Tang, D, Xiao, G, Xing, L, Boyce, BF, Chen, D (2014) Chondrocyte beta-catenin signaling regulates postnatal bone remodeling through modulation of osteoclast formation in a murine model. *ARTHRITIS RHEUMATOL* **66**(1)**:** 107-120.

Wang, HD, Shi, YM, Li, L, Guo, JD, Zhang, YP, Hou, SX (2013) Treatment with resveratrol attenuates sublesional bone loss in spinal cord-injured rats. *Br J Pharmacol* **170**(4)**:** 796-806.

Wang, W, Bai, J, Zhang, W, Ge, G, Wang, Q, Liang, X, Li, N, Gu, Y, Li, M, Xu, W, Yang, H, Xu, Y, Geng, D, Zhou, J (2020) Protective Effects of Punicalagin on Osteoporosis by Inhibiting Osteoclastogenesis and Inflammation via the NF-κB and MAPK Pathways. *FRONT PHARMACOL* **11**.

Wang, YX, Rudnicki, MA (2011) Satellite cells, the engines of muscle repair. *Nat Rev Mol Cell Biol* **13**(2)**:** 127-133.

Wu, F, Li, H, Jin, L, Li, X, Ma, Y, You, J, Li, S, Xu, Y (2013) Deer antler base as a traditional Chinese medicine: a review of its traditional uses, chemistry and pharmacology. *J ETHNOPHARMACOL* **145**(2)**:** 403-415.

Xiang, L, Liang, C, Zhen-Yong, K, Liang-Jun, Y, Zhong-Liang, D (2012) BMP9-induced osteogenetic differentiation and bone formation of muscle-derived stem cells. *J Biomed Biotechnol* **2012:** 610952.

Xiong, R, Li, Y, Zheng, K, Zhang, T, Gao, M, Li, Y, Lian, Y, Chen, D, Hu, C (2019) Er Shen Wan extract alleviates polyuria and regulates AQP 2 and AVPR 2 in a rat model of spleen-kidney Yang

deficiency-induced diarrhea. *BIOMED PHARMACOTHER* **110:** 302-311.

Xu, H, Xu, J, Chen, F, Liu, T, Li, J, Jiang, L, Jia, Y, Hu, C, Gao, Z, Gan, C, Hu, L, Wang, X, Sheng, J (2020) Acanthopanax senticosus aqueous extract ameliorates ovariectomy-induced bone loss in middle-aged mice by inhibiting the receptor activator of nuclear factor-kappaB ligand-induced osteoclastogenesis. *FOOD FUNCT* **11**(11)**:** 9696-9709.

Yan, Y, Tang, D, Chen, M, Huang, J, Xie, R, Jonason, JH, Tan, X, Hou, W, Reynolds, D, Hsu, W, Harris, SE, Puzas, JE, Awad, H, O'Keefe, RJ, Boyce, BF, Chen, D (2009) Axin2 controls bone remodeling through the beta-catenin-BMP signaling pathway in adult mice. *J CELL SCI* **122**(Pt 19)**:** 3566-3578.

Yuan, Q, Zhang, J, Xiao, C, Harqin, C, Ma, M, Long, T, Li, Z, Yang, Y, Liu, J, Zhao, L (2020) Structural characterization of a low-molecular-weight polysaccharide from Angelica pubescens Maxim. f. biserrata Shan et Yuan root and evaluation of its antioxidant activity. *Carbohydr Polym* **236:** 116047.

Zhang, Y, Jiang, J, Shen, H, Chai, Y, Wei, X, Xie, Y (2017) Total flavonoids from Rhizoma Drynariae (Gusuibu) for treating osteoporotic fractures: implication in clinical practice. *Drug Des Devel Ther* **11:** 1881-1890.

Zheng, H, He, B, Wu, T, Cai, J, Wei, J (2020) Extraction, purification and anti-osteoporotic activity of a polysaccharide from Epimedium brevicornum Maxim. in vitro. *INT J BIOL MACROMOL* **156:** 1135-1145.

Zhou, Y, Wang, C, Si, J, Wang, B, Zhang, D, Ding, D, Zhang, J, Wang, H (2020) Melatonin up-regulates bone marrow mesenchymal stem cells osteogenic action but suppresses their mediated osteoclastogenesis via MT2 -inactivated NF-kappaB pathway. *Br J Pharmacol* **177**(9)**:** 2106-2122.

Zou, YF, Zhang, YY, Fu, YP, Inngjerdingen, KT, Paulsen, BS, Feng, B, Zhu, ZK, Li, LX, Jia, RY, Huang, C, Song, X, Lv, C, Ye, G, Liang, XX, He, CL, Yin, LZ, Yin, ZQ (2019) A Polysaccharide Isolated from Codonopsis pilosula with Immunomodulation Effects Both In Vitro and In Vivo. *MOLECULES* **24**(20).

FIGURE 1 | ISTKF mediates β-catenin to promote myogenic differentiation. (**A**) The muscle coefficient ratio of the four groups. (**B**) Statistical results of muscle coefficient ratio of four groups. (**C**) β-catenin immunohistochemical staining of the left calf muscle of the four groups. Retest of the knockout efficiency of the TM group. Bar, 50 μm. (**D**) Related quantitative analysis of β-catenin immunohistochemical staining. Results are shown as mean±SEM (n=10). **P*<0.05, ***P*<0.01, ****P*<0.001. (**E**) Western blot analysis of muscle β-catenin knockout efficiency and detection of myogenic differentiation indicators MEF2C and MyoD1. (**F**) Related quantitative analysis of Western blot. (**G**) Immunofluorescence staining (MyoD+BrdU) of the posterior tibial muscle on the model side at 7 dpf. Bar, 20 μm.

FIGURE 2 | ISTKF mediates β-catenin to regulate SMSCs and promote myogenic differentiation. (**A**) H&E staining of the left calf muscle (cross-section). Bar, 50 μm. (**B**) H&E staining of the left calf muscle (longitudinal section). Bar, 50 μm. (**C**) Masson's staining of left calf muscles (cross-section). Bar, 50 μm. (**D**) Masson's staining of left calf muscles (longitudinal section). Bar, 50 μm. (**E**) Immunofluorescence staining (Pax7+Sca1) of the posterior tibial muscle on the modeled side at 7 dpf. Bar, 20 μm. (**F**) Immunofluorescence staining (Pax7+BrdU) of the posterior tibial muscle on the modeled side at 7 dpf. Bar, 20 μm. ISTKF promotes the proliferation activity of SMSCs in skeletal muscle.

FIGURE 3 | ISTKF mediates β-catenin to promote OPF healing. (**A**) X-ray scan of the left tibia at 7 dpf and 14 dpf. (**B**) Micro-CT 3D reconstruction and quantitative analysis at 7 dpf. Bar, 1 mm. (**C**) Micro-CT 3D reconstruction and quantitative analysis at 14 dpf. Bar, 1 mm. Analysis of tibial

fracture site by H&E staining, treated for 7 dpf (**D**) and 14 dpf (**E**). Bar, 500 μm. Analysis of tibial fracture site by Alcian Blue/hematoxylin and orange G staining after treatment for 7 dpf (**F**) and 14 dpf (**G**). Bar, 500 μm. Analysis of tibial fracture site by Safranin-fixed green staining, treated for 7 dpf (**H**) and 14 dpf (**I**). Bar, 500 μm.

FIGURE 4 | ISTKF mediates β-catenin to regulate osteogenic differentiation of SMSCs to promote OPF healing. (**A**) Immunohistochemical β-catenin staining of the fracture sites of each groups at 7 dpf and 14 dpf. Bar, 50 μm. (**B**) Immunohistochemical OPG staining of the fracture sites in each group at 7 dpf and 14 dpf. Bar, 50 μm. (**C**) Immunofluorescence staining of tibial fracture site (Pax7+Sca1). Bar, 50 μm. (**D**) Immunofluorescence staining of tibial fracture site (Pax7+BrdU). Bar, 50 μm. ISTKF mobilizes SMSCs to migrate to the callus for expression and upregulates the expression of osteoblasts, thereby promoting callus formation and fracture healing.

FIGURE 5 | UPLC-Q-TOF/MS analysis of ISTK ingredients. (**A**) Representative ion chromatogram of ISTK in the negative mode. (**B**) Representative ion chromatogram of ISTK in the positive mode. (**C**) The chemical structure of the higher peak component in the ISTKF.

FIGURE 6 | ISTKF regulates skeletal muscle satellite cells and plays a vital role in the healing of osteoporotic fractures mediated by β-catenin. When β-catenin is knocked out in SMSCs, sarcopenia and osteopenia are observed. Conversely, when β-catenin is promoted by ISTKF, it promotes fracture healing and skeletal muscle fiber remodeling. CP: *Codonopsis pilosula*, RD: *Rhizoma drynariae*, AS: *Acanthopanax senticosus*, EBM: *Epimedium brevicornum* Maxim, SMB:

Slauia miltiorrhiza Bunge, RAP: Root of *Angelicae pubescens*.

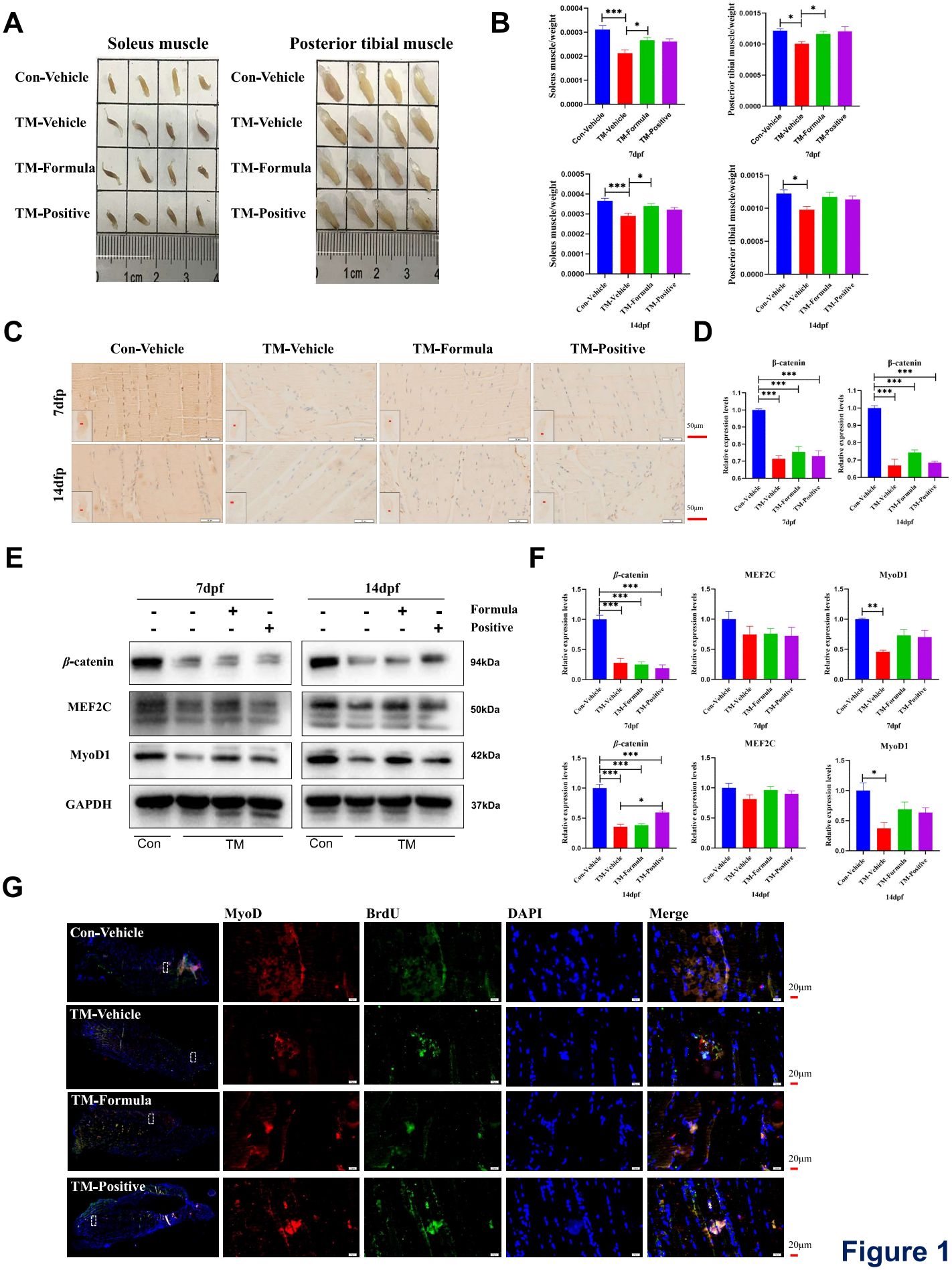
A
Soleus muscle
Posterior tibial muscle
Con-Vehicle
TM-Vehicle
TM-Formula
TM-Positive
1cm 2 3 4
B
Soleus muscle/weight
Posterior tibial muscle/weight
7dpf
14dpf
C
7dfp
14dfp
50μm
D
β-catenin
Relative expression levels
E
7dpf
14dpf
Formula
Positive
β-catenin
MEF2C
MyoD1
GAPDH
94kDa
50kDa
42kDa
37kDa
Con
TM
F
β-catenin
MEF2C
MyoD1
G
MyoD
BrdU
DAPI
Merge
20μm

Figure 1

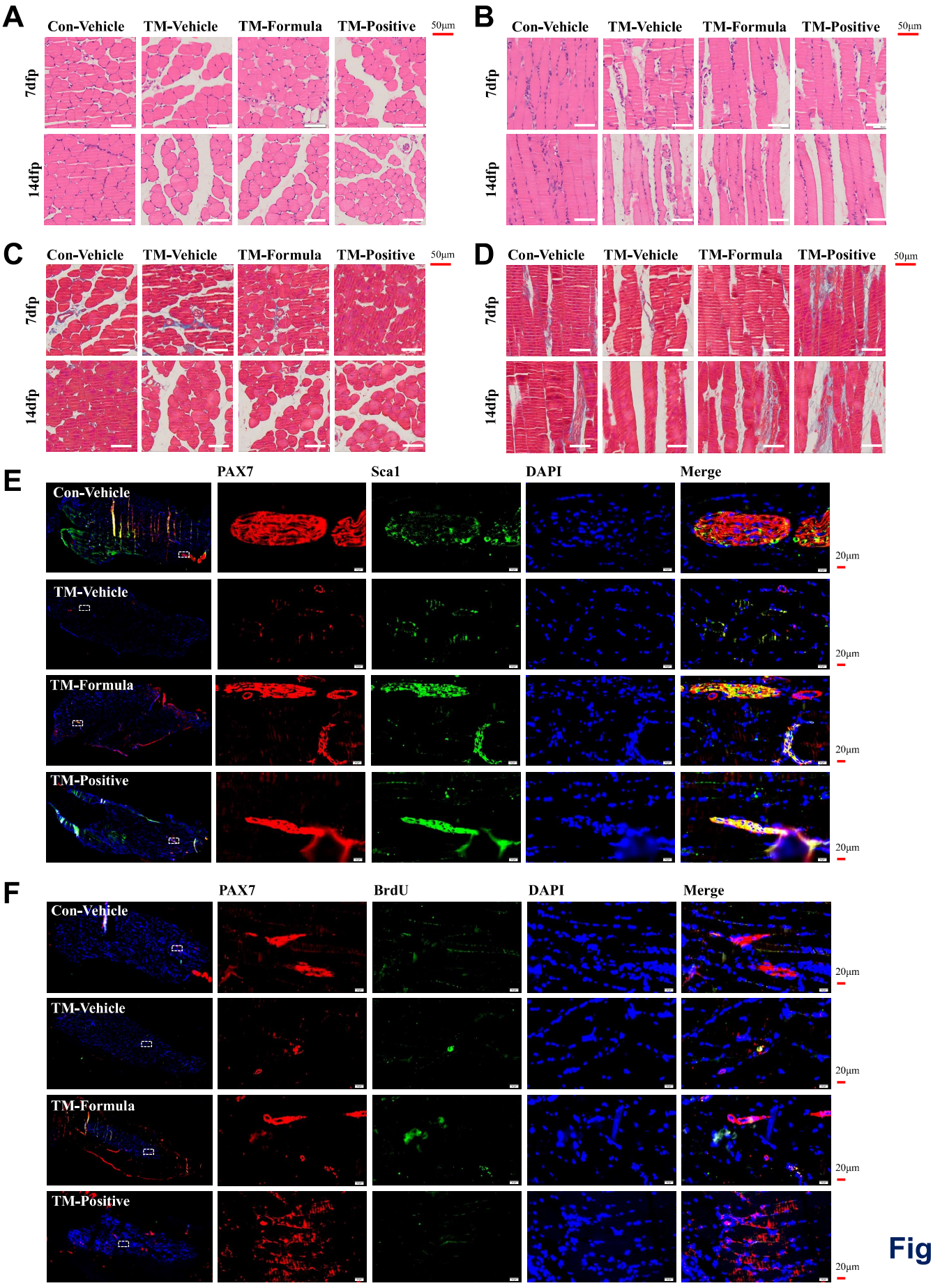
A
Con-Vehicle
TM-Vehicle
TM-Formula
TM-Positive
50μm
7dfp
14dfp
B
Con-Vehicle
TM-Vehicle
TM-Formula
TM-Positive
50μm
7dfp
14dfp
C
Con-Vehicle
TM-Vehicle
TM-Formula
TM-Positive
50μm
7dfp
14dfp
D
Con-Vehicle
TM-Vehicle
TM-Formula
TM-Positive
50μm
7dfp
14dfp
E
PAX7
Sca1
DAPI
Merge
Con-Vehicle
TM-Vehicle
TM-Formula
TM-Positive
20μm
F
PAX7
BrdU
DAPI
Merge
Con-Vehicle
TM-Vehicle
TM-Formula
TM-Positive
20μm

Figure 2

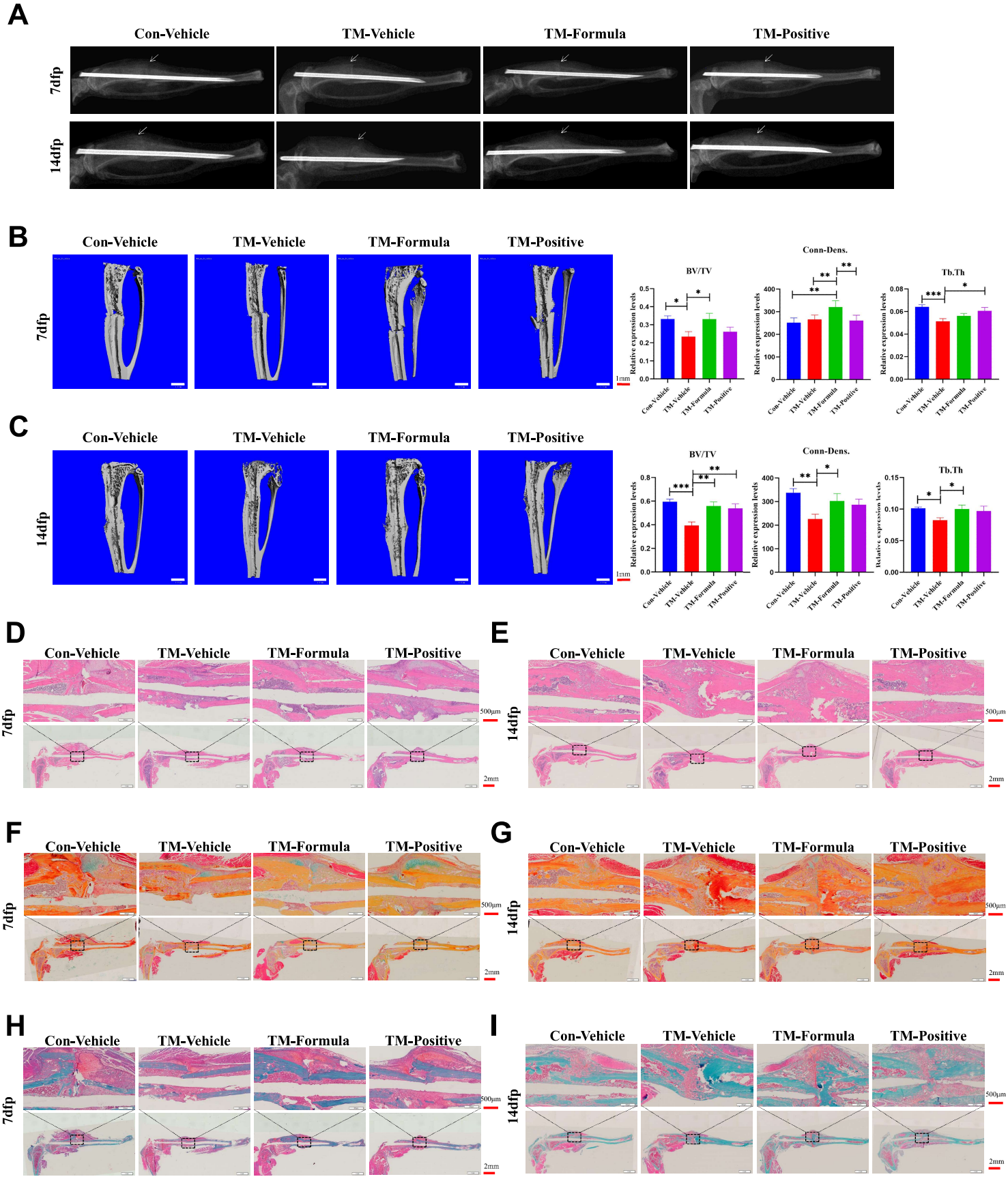
A
Con-Vehicle
TM-Vehicle
TM-Formula
TM-Positive
7dfp
14dfp
B
C
BV/TV
Conn-Dens.
Tb.Th
Relative expression levels
1mm
D
E
F
G
H
I
500μm
2mm

Figure 3

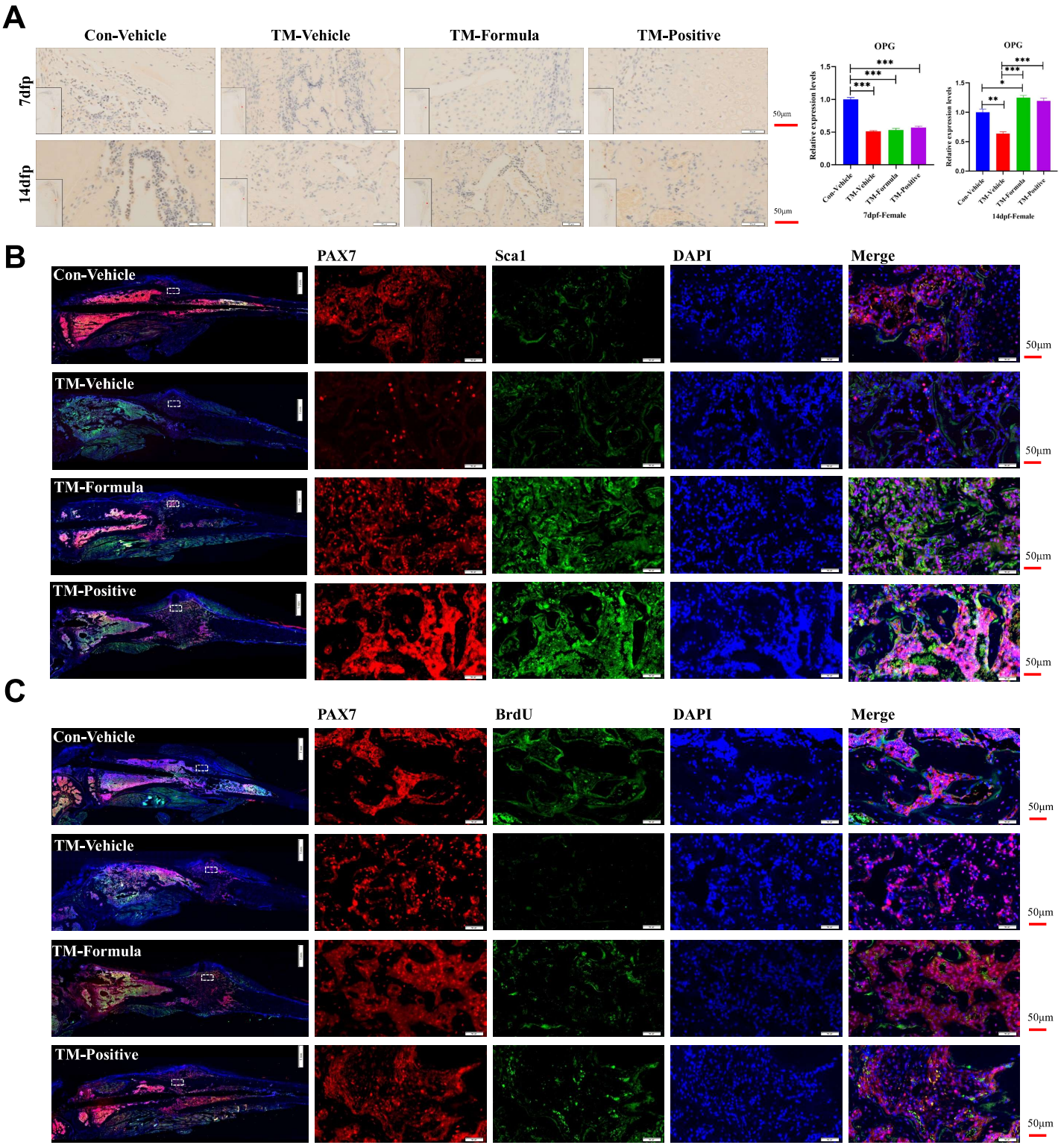
A
Con-Vehicle
TM-Vehicle
TM-Formula
TM-Positive
7dfp
14dfp
50μm
OPG
Relative expression levels
7dpf-Female
14dpf-Female
B
PAX7
Sca1
DAPI
Merge
C
BrdU

Figure 4

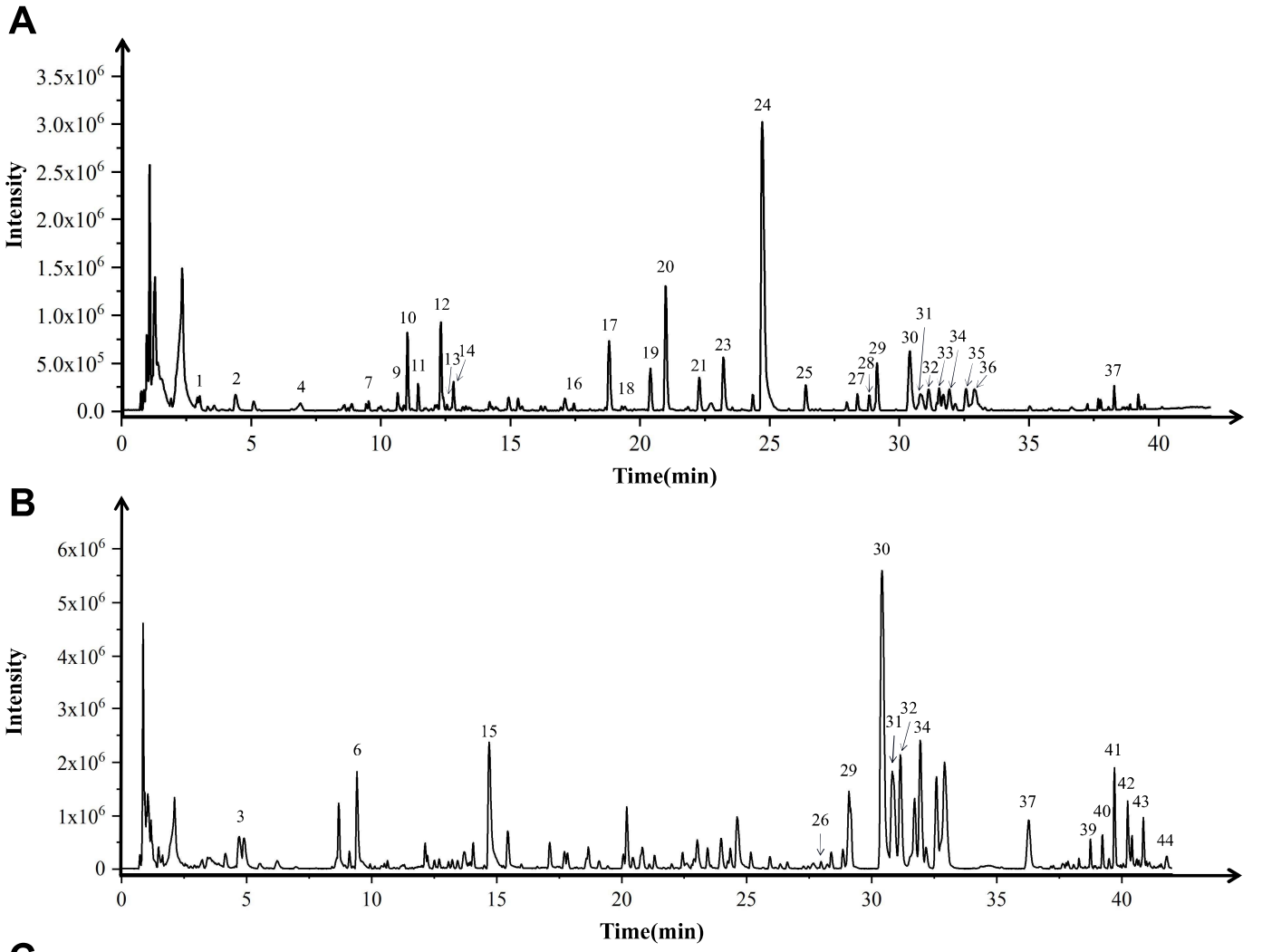
A
Intensity
Time(min)
B
Intensity
Time(min)
C
Caffeic acid 3-O-β-D-glucoside
Chlorogenic acid
Neoeriocitrin
Naringin
Salvianolic acid B
Icariin
Codonopsine
Magnoflorine
Angelol A
Angelol C
Angelol E
Angelol B
Angenomalin
Osthole

Figure 5

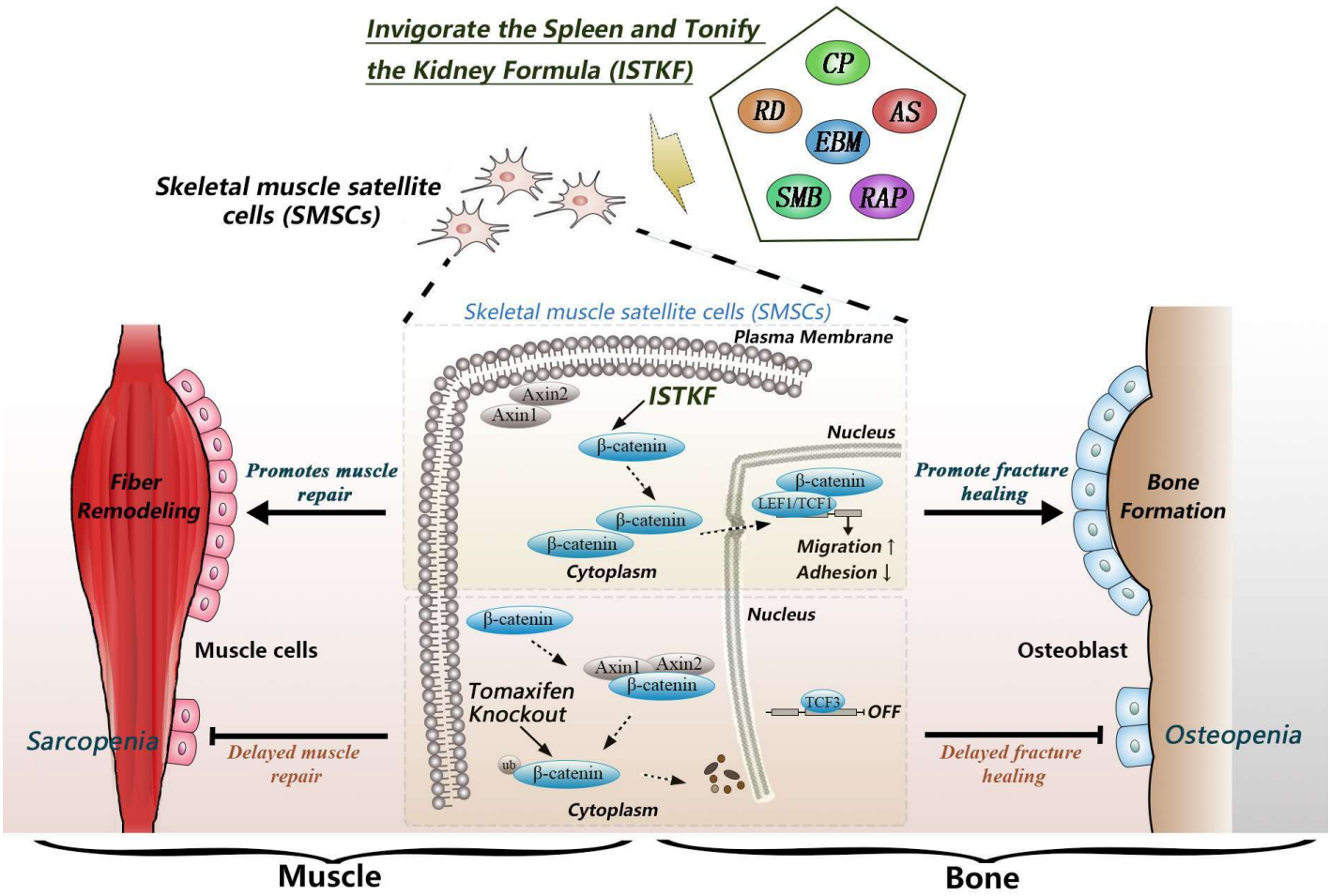
Invigorate the Spleen and Tonify the Kidney Formula (ISTKF)
CP
RD
AS
EBM
SMB
RAP
Skeletal muscle satellite cells (SMSCs)
Skeletal muscle satellite cells (SMSCs)
Plasma Membrane
Axin2
Axin1
ISTKF
β-catenin
Nucleus
β-catenin
LEF1/TCF1
β-catenin
β-catenin
Migration ↑
Adhesion ↓
Cytoplasm
Fiber Remodeling
Promotes muscle repair
Promote fracture healing
Bone Formation
β-catenin
Nucleus
Axin1
Axin2
β-catenin
Tomaxifen Knockout
TCF3
OFF
Muscle cells
Osteoblast
Sarcopenia
Delayed muscle repair
ub
β-catenin
Cytoplasm
Delayed fracture healing
Osteopenia
Muscle
Bone

Figure 6

TABLE 1 | Prescription of Invigorate the Spleen and Tonify the Kidney (ISTK).

Latin name	Chinese name	Amount (g)	Lot No.	Place of origin	Company
Codonopsis pilosula.	Dangshen	12	190822-1	Shanxi, China	Shanghai WanShiCheng Chinese Medicine Co. Ltd.
Rhizoma Drynariae.	Gusuibu	9	2019062802	Chongqing, China	Shanghai DeHua Chinese Medicine Co. Ltd.
Acanthopanax senticosus.	Ciwujia	12	20200811	Changbai, China	Linjiang Tranquil Local Product Shop
Epimedium brevicornum Maxim.	Yinyanghuo	9	2019082006	Gansu, China	Shanghai DeHua Chinese Medicine Co. Ltd.
Slauia miltiorrhiza Bunge.	Danshen	12	200706	Shandong, China	Shanghai Hongqiao traditional Chinese medicine decoction pieces Co., Ltd.
Root of Angelicae Pubescens.	Duhuo	9	20200515-1	Hubei, China	Shanghai WanShiCheng Chinese Medicine Co. Ltd.

The voucher specimens were deposited at Longhua Hospital, affiliated with Shanghai University of TCM. The voucher numbers were as follows: Codonopsis pilosula (No.190822-1-Tang), Rhizoma Drynariae (NO.22019062802-Tang), Acanthopanax senticosus (No.20200811-Tang), Epimedium brevicornum Maxim (No.2019082006-Tang), Slauia miltiorrhiza Bunge (No.200706-Tang), Angelicae Pubescentis Radix (No.20200515-1-Tang).

TABLE 2 | The mass information and source of identified compounds in Invigorate the Spleen and Tonify the Kidney (ISTK) by high-performance liquid chromatography quadrupole time-of-flight mass spectrometry (HPLC–Q-TOF).

No	Identification	Formula	Mass	Rt(min)	Error(ppm)	Classification
1	Uridine*	$C_9H_{12}N_2O_6$	244.07	3.00	1.1	/
2	cGMP	$C_{10}H_{12}N_5O_7P$	345.05	4.34	1.4	/
3	Adenosine*	$C_{10}H_{13}N_5O_4$	267.10	4.70	-3.2	/
4	Guanosine*	$C_{10}H_{13}N_5O_5$	283.09	6.91	0.8	/
5	Danshensu*	$C_9H_{10}O_5$	198.05	8.86	0.9	Slauia miltiorrhiza Bunge.(SMB)
6	Codonopsine	$C_{14}H_{21}NO_4$	267.15	9.41	1.3	Codonopsis pilosula.(CP)
7	Protocatechuicacid-3-O-glucoside	$C_{13}H_{16}O_9$	316.08	9.43	1.5	SMB
8	3,4-Dihydroxybenzaldehyde*	$C_7H_6O_3$	138.03	10.28	0.8	Epimedium brevicornum Maxim.(EBM)、SMB、Acanthopanax senticosus.(AS)
9	Neochlorogenic acid*	$C_{16}H_{18}O_9$	354.10	10.66	2.0	CP、EBM
10	Caffeic acid 3-O-β-D-glucoside	$C_{15}H_{18}O_9$	342.10	11.00	3.9	SMB、Rhizoma Drynariae.(RD)
11	Eleutheroside B2	$C_{23}H_{30}O_{14}$	530.16	11.43	2.5	AS
12	Chlorogenic acid*	$C_{16}H_{18}O_9$	354.10	12.31	3.4	CP、EBM
13	Syringin*	$C_{17}H_{24}O_9$	372.14	12.39	1.6	CP、AS
14	Cryptochlorogenic acid*	$C_{16}H_{18}O_9$	354.10	12.80	2.6	CP、EBM
15	Magnoflorine*	$C_{20}H_{24}NO_4^+$	342.17	14.82	-0.3	EBM
16	Eleutheroside E*	$C_{34}H_{46}O_{18}$	742.27	17.45	1.8	AS
17	Neoeriocitrin*	$C_{27}H_{32}O_{15}$	596.17	18.78	3.5	RD
18	Nodakenin*	$C_{20}H_{24}O_9$	408.14	20.36	3.1	Root of Angelicae Pubescens.(RAP)
19	Salvianolic acid I	$C_{27}H_{22}O_{12}$	538.11	20.40	2.2	SMB
20	Naringin*	$C_{27}H_{32}O_{14}$	580.18	20.98	4.5	RD
21	Rosmarinic acid*	$C_{18}H_{16}O_8$	360.08	22.28	3.6	SMB
22	Salvianolic acid E*	$C_{36}H_{30}O_{16}$	718.15	22.28	1.7	SMB
23	Lithospermic acid*	$C_{27}H_{22}O_{12}$	538.11	23.19	1.3	SMB
24	Salvianolic acid B*	$C_{36}H_{30}O_{16}$	718.15	24.71	2.5	SMB
25	Salvianolic acid Y*	$C_{36}H_{30}O_{16}$	718.15	26.38	2.9	SMB
26	Epimedin A	$C_{39}H_{50}O_{20}$	838.29	27.97	0.4	EBM
27	Epimedin B	$C_{38}H_{48}O_{19}$	808.28	28.37	2.9	EBM
28	Epimedin C*	$C_{39}H_{50}O_{19}$	822.29	28.82	1.8	EBM
29	Icariin*	$C_{33}H_{40}O_{15}$	676.24	29.13	3.9	EBM
30	Angelol A*	$C_{20}H_{24}O_7$	376.15	30.40	4.5	RAP
31	Angelol C	$C_{20}H_{26}O_7$	378.17	30.84	0.1	RAP
32	Angelol E	$C_{20}H_{26}O_7$	378.17	31.14	0.1	RAP
33	Anhydroicaritin-3-O-rhamnodide(1-2)-furanacid-7-O-glucoside	$C_{39}H_{48}O_{19}$	820.28	31.53	3.0	EBM
34	Angelol B	$C_{20}H_{24}O_7$	376.15	31.94	1.1	RAP
35	Angelol D	$C_{20}H_{24}O_7$	376.15	32.58	0.0	RAP
36	Angelol F	$C_{20}H_{26}O_7$	378.17	32.91	0.7	RAP
37	Angenomalin	$C_{14}H_{12}O_3$	228.08	36.25	-1.5	RAP
38	Baohuoside I*	$C_{27}H_{30}O_{10}$	514.18	38.28	3.9	EBM
39	3-Hydroxytanshinone IIB	$C_{19}H_{18}O_5$	326.12	38.73	-2.5	SMB
40	Isocryptotanshinone*	$C_{19}H_{20}O_3$	296.14	39.21	0.5	SMB
41	Osthole*	$C_{15}H_{16}O_3$	244.11	39.69	-3.4	RAP
42	Cryptotanshinone	$C_{19}H_{20}O_3$	296.14	40.84	0.5	SMB
43	Tanshinone I*	$C_{18}H_{12}O_3$	276.08	40.93	-1.6	SMB
44	Tanshinone II A*	$C_{19}H_{18}O_3$	294.13	42.16	0.0	SMB

*Identified with the reference compounds.

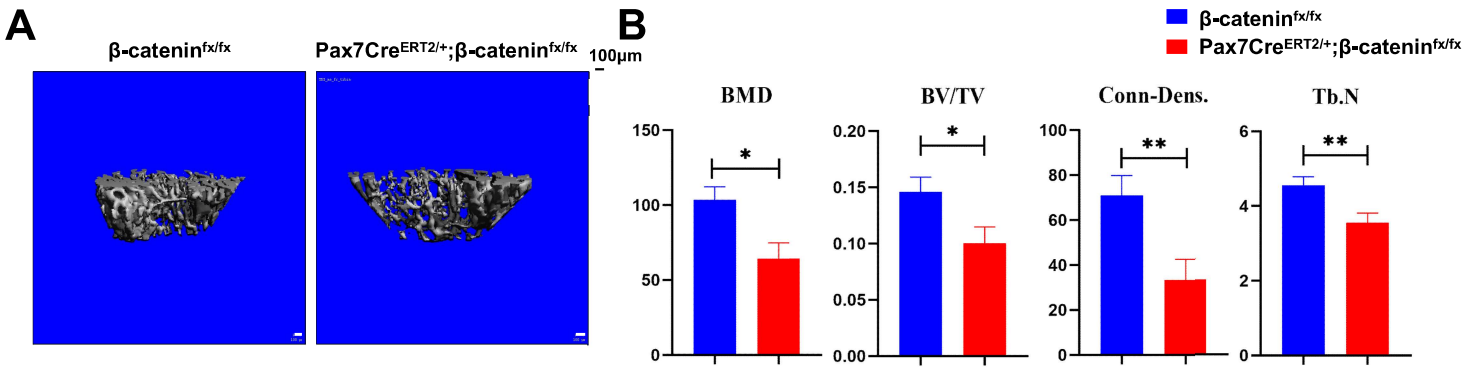

Supplemental figure 1

Supplemental figure 1 | (**A**)Through the Micro-CT detection of the tibia, it was found that Pax7-Cre$^{ERT2/+}$;β-catenin$^{fx/fx}$ transgenic mice decreased bone mass. (**B**)Pax7-Cre$^{ERT2/+}$;β-catenin$^{fx/fx}$ transgenic mice have significantly lower BMD than β-catenin$^{fx/fx}$ transgenic mice, $^{**}P<0.01$; Also, BV/TV, Conn-Dens and Tb.N is also lower than β-catenin$^{fx/fx}$ transgenic mice, $^{*}P<0.05$.

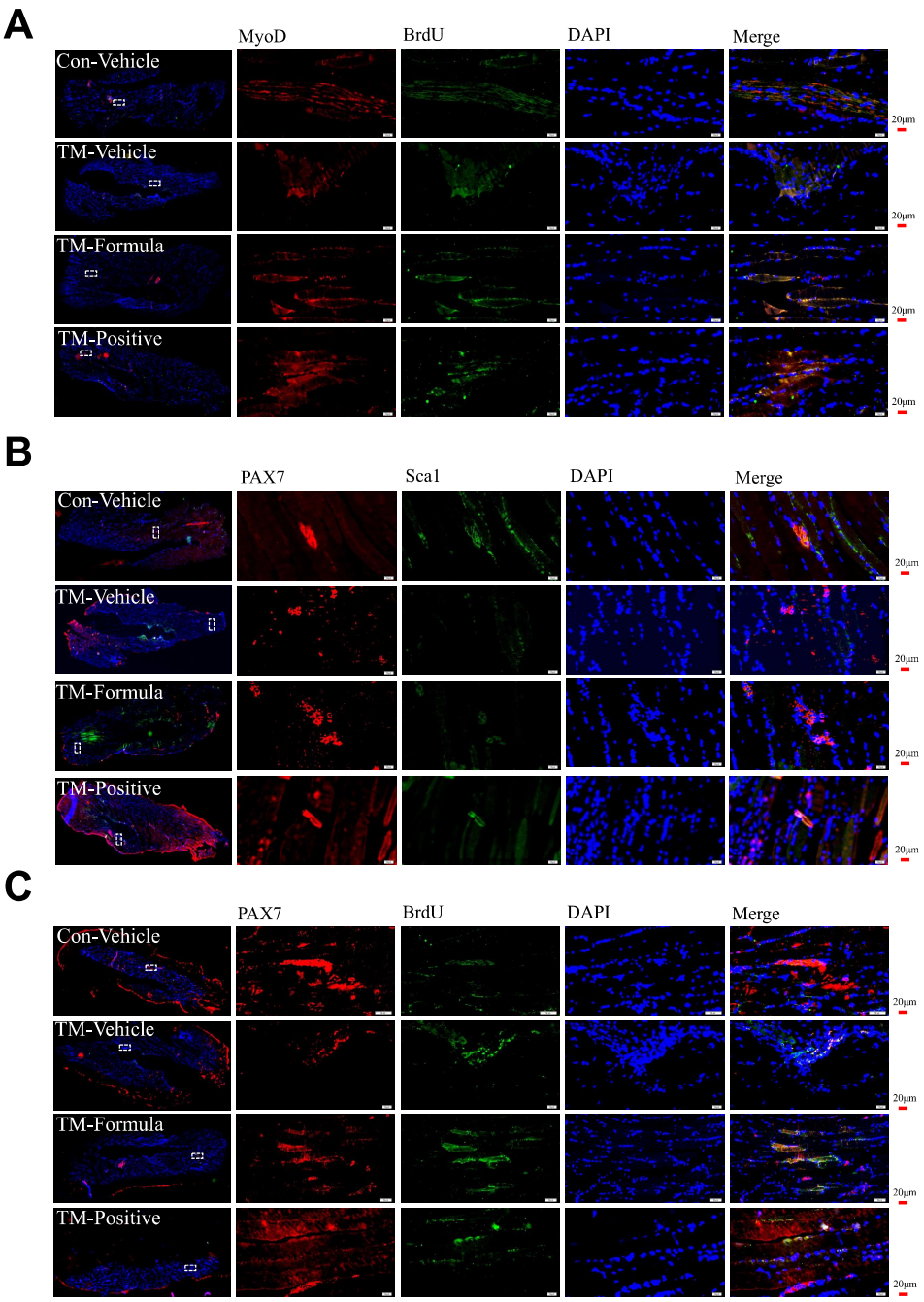

Supplemental figure 2

Supplemental figure 2 | ISTKF mediates β-catenin to regulate SMSCs to promote myogenic differentiation. (**A**) Immunofluorescence staining (MyoD+BrdU) of the posterior tibial muscle on the model side at 14 dpf. Bar, 20 μm. (**B**) Immunofluorescence staining (Pax7+Sca1) of the posterior tibial muscle on the modeled side at 14 dpf.. Bar, 20 μm. (**C**) Immunofluorescence staining (Pax7+BrdU) of the posterior tibial muscle on the modeled side at 14 dpf.. Bar, 20 μm. ISTKF can effectively promote the proliferation activity of SMSCs in skeletal muscle.